FINITE ELEMENT ANALYSIS OF YIELD FUNCTIONS OF KELVIN FOAMS WITH OPEN CELLS

By

Beiqing Huang

RECOMMENDED:

Chuen-Sen Lin

Advisory Committee Chair

Head, Mechanical Engineering Department

APPROVED:

Dean, College of Science, Engineering and Mathematics

Dean of the Graduate School

12-4-01

Date

FINITE ELEMENT ANALYSIS OF YIELD FUNCTIONS OF KELVIN FOAMS WITH OPEN CELLS

A

THESIS

Presented to the Faculty

of the University of Alaska Fairbanks

in Partial Fulfillment of the Requirements

for the Degree of

MASTER OF SCIENCE

By

Beiqing Huang, B.S.

Fairbanks, Alaska

December 2001

Abstract

Proper design of foams requires an understanding of the response of the materials to stress. This thesis, based on finite element analysis, provides numerical solutions in modeling the yield behavior of Kelvin foams.

The FEA model, representing a complicated unit cell, was calculated and meshed. C++ programs were designed and implemented to generate meshes for unit cells. Finite element analyses were performed for many cases. Multiple methods were employed for the determination of yield points which form yield surfaces. Comparisons between several results have been made. Our FEA results, Zhang's function and Gibson's theory show good agreements except some differences under hydrostatic loading. A conclusion can be made: besides the void fraction and the yield strength of the wall material, the structure of foams also has a significant effect on the yield behavior of foams. Yield surfaces normalized by the uniaxial tensile strength of foams are more reasonable.

Contents

List of Figures

List of Tables

Acknowledgements

I would like to thank Dr. Jonah Lee, professor of Mechanical Engineering, my graduate advisor and chairman of the graduate committee, for his continuous academic guidance, support and encouragement.

I would also like to thank my graduate committee members, Dr. Chuen-Sen Lin and Dr. Hong Liang, professors of Department of Mechanical Engineering, University of Alaska Fairbanks, for their valuable technical tutorial.

I would also like to thank my wife, Yingying Wang, for her understanding and endless support.

Chapter 1

Introduction

Materials with a porous structure are increasingly used in engineering applications. Aluminum, paper and polymeric honeycombs and foams are used as cores for high-performance sandwich panels; plastic and metal foams absorb energy in packaging and safety padding; and natural cellular materials — particularly woods — are widely used in structures (Gibson, 1989). A proper design requires the knowledge of the response of these materials to multiaxial states of stress.

Porous structures are usually made of repetitive, representative micro-units called unit cells. There are two kinds of microstructures for porous structures: closed cells and open cells. We distinguish foams, which have three-dimensional, polyhedral cells from honeycombs, with their two-dimensional, prismatic cells.

The yield behavior of the closed cell structure has been widely studied (Tvergaad, 1990), which is greatly facilitated by the development of the so called Gurson's model (Gurson, 1977). Based on a single unit cell that statistically

represents an aggregate of voids and matrix, Gurson derived an approximate yield criterion of void containing (cellular material) metals using a simple rigid-plastic material model and the upper bound theorem of plasticity. In Gurson's model, the yielding of the matrix of the unit cell is described by the von Mises yield criterion and the plastic dilatation of the porous material is solely due to the presence of void and its growth. Later studies by Lee and Oung (2000) and Jeong (1995) contributed further to the development of more general yield surfaces, characterizing the pressure-dependency of the materials. Lee and Oung studied the influence of the pressure-dependency of the matrix of a unit cell on the yield criteria and the related flow rules of a class of glassy polymers. In their model, the yielding of the matrix obeys the modified von Mises yield criterion (Raghava et al., 1973) and the plastic dilatation of the glassy polymers is the result of both the void growth and the pressure-dependency of the matrix. Because of the complicated geometry, the modeling of the linear elastic behavior of open cell structures such as foams, and the failure studies of the open cell structure are still in their infancy. An examination of the yield behavior of the open cell materials under multiaxial loads was carried out by extending, using dimensional arguments, the analysis for honeycombs (Gibson et al., 1989). Honeycombs are always anisotropic, while open cell materials can be isotropic or anisotropic depending on the strut (the component of the unit cell) orientations in the materials. In Gibson's model, the open unit cell was simplified as a three dimensional frame structure. A yield function was

obtained approximately by analyzing the development of the plastic hinges in the honeycomb (two dimensional unit cell) first and then extended to the three dimensional frame (foams). The extension of the yield behavior of honeycombs by Ashby and Gibson may not be applicable to some open cell microstructures such as the ones discussed later in the current thesis. Contrast to yielding, another competing failure mechanism of the open cell materials is buckling, which is related to the bending stiffness and the orientation of each strut composing the unit cell frame. Gibson's (1989) four strut mode is a good starting point to observe the buckling behavior of the open cell materials but not necessary a sophisticated model to describe the failure surface. Recently, Deshpande and Fleck (2001) have done research on the multiaxial yield behavior of ploymer foams theoretically and experimentally.

"In real engineering design, the stress state is often a complex one. Only limited experimental data exist on the multiaxial deformation of polymeric foams. The presence of experimental scatter and the paucity of tensile loading states in studies have made it very difficult to establish unambiguously the shape of the yield surfaces" (Deshpande 2001). With the development of computer technology, the numerical method, finite element method, has become widely used in recent years. Compared to experimental method, the numerical method may be less costly, more suitable and practical for very complicated geometry and boundary conditions.

In this thesis, a well-known porous structure – open-cell Kelvin foam is used.

A representative unit cell is chosen for the analysis, and geometrical calculations for the very complicated unit cell have been done. Due to the complex geometry of the unit cell and a great amount of meshing needed for the analysis, C++ programs for generating unit cell meshes were designed and implemented. They greatly simplified the meshing of the unit cell and can be reused for other unit cells in future studies. Finite element analyses for many cases (different void fractions and different loads) were performed and many numerical results were acquired. And finally, comparisons between numerical simulation and some existing analytical results were conducted. Most of the analytical and numerical calculations for geometries were done by using Mathematica. The commercial finite element code ABAQUS (Hibbit, Karlsson & Sorensen Inc., 1999), which is available at the Arctic Region Supercomputing Center, was used in this study.

Chapter 2

Unit Cell of Open Foams Using the Kelvin Model

2.1 Open foams using the Kelvin model

In this thesis, we consider a perfectly ordered foam whose geometry is based on the regular tetrakaidecahedron shown in Figure 2.1. We refer this idealized structure as an open-cell Kelvin foam following the classic work on soap froth geometry (Thomson, 1887). The Kelvin cell is the only polyhedral bubble known that fills space to form a dry soap foam (one that contains very little liquid) with perfect order; i.e., all cells have identical shape and orientation, only their positions differ. Other polyhedra that fill space, such as cubes, do not satisfy the minimal energy conditions embodied in Plateau's laws (Plateau, 1873). The basic model consists of 36 struts which construct flat faced 14-hedra

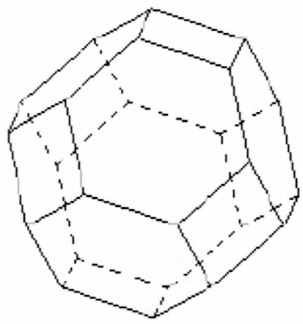

Figure 2.1: A 14-hedra of the flat faced Kelvin BBC foam

(tetrakaidecahedra), six squares and eight hexagons. These 14-hedra pack in a body-centered cubic (BCC) arrangement. All 14-hedra have the same size with cubic symmetry. The stiffness of the resulting cellular solid has cubic symmetry. Figure 2.2 shows a projection in one of the three axial directions. All three projections from three axial directions are identical.

2.1.1 Unit cell for foams using the Kelvin model

2.1.1.1 Unit cell

A unite cell is a repetitive, representative unit that makes up the microstructure. The foam using the Kelvin model can be further considered to be made of smaller unit cells. The unit cell is composed of 12 half-lengthed and 6 complete struts. Figure 2.3 shows a typical cubic unit cell including the struts and the void.

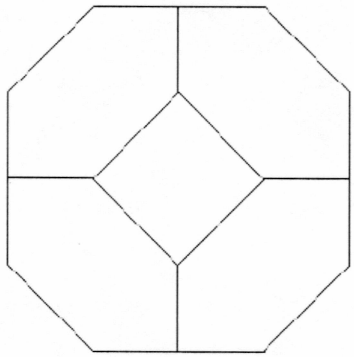

Figure 2.2: The projection of the 14-hedra of the Kelvin BCC foam

Generally, the void fraction (f) is used to characterize a unit cell. It is defined as the volume of the void divided by the volume of the entire unit cell and is related to the relative density (ϕ) of the unit cell,

$$\phi = 1 - f, \tag{2.1}$$

such that $\phi = 1.0$ for solid matrices and $\phi = 0.0$ for void matrices.

2.1.1.2 Calculations of coordinates of end points of struts

Figure 2.4 shows struts of the unit cell and some imaginary lines for calculation. The angle between the plane MNOPQR and the plane which includes line AM and line MR is α. Suppose the length of one strut is 1,

$\frac{\alpha}{2} = \arcsin(\frac{AS}{ST})$;

$AS = \frac{\sqrt{2}}{2}$; $ST = \frac{\sqrt{3}}{2}$;

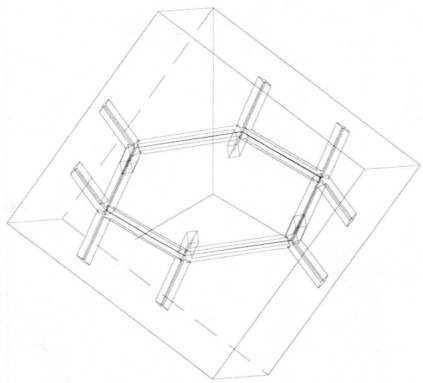

Figure 2.3: The unit cell for foams using Kelvin model

$\alpha = 2\arcsin(AS/ST) = 2\arcsin(\sqrt{\frac{2}{3}}) = 109.471°;$

$x_A = \frac{\sqrt{3}}{2} - \frac{\sqrt{3}}{4}\cos\alpha;\ y_A = \frac{1}{2} + \frac{1}{4};\ z_A = \frac{\sqrt{3}}{4}\sin\alpha;$

$x_F = \frac{\sqrt{3}}{2} - \frac{\sqrt{3}}{4}\cos\alpha;\ y_F = -\frac{3}{4};\ z_F = \frac{\sqrt{3}}{4}\sin\alpha;$

$x_B = x_F\cos 120° - y_F\sin 120°;\ y_B = x_F;$

$x_C = x_A\cos 120° - y_A\sin 120°;\ y_C = x_A\sin 120° + y_A\cos\alpha;\ z_C = \frac{\sqrt{3}}{4}\sin\alpha;$

$x_D = x_F\cos 240° - y_F\sin 240°;\ y_D = x_F\sin 240° + y_F\cos 240°;\ z_F = \frac{\sqrt{3}}{4}\sin\alpha;$

$x_E = x_A\cos 240° - y_A\sin 240°;\ y_E = x_A\sin 240° + y_A\cos 240°;\ z_E = \frac{\sqrt{3}}{4}\sin\alpha;$

$x_G = x_F\cos(-60°) - y_F\sin(-60°);\ y_G = x_F\sin(-60°) + y_F\cos(-60°);$

$z_G = -\frac{\sqrt{3}}{4}\sin\alpha;$

$x_H = x_F\cos 60° - y_F\sin 60°;\ y_H = x_F\sin 60° + y_F\cos 60°;\ z_H = \frac{\sqrt{3}}{4}\sin\alpha;$

$x_I = x_A\cos 60° - y_A\sin 60°;\ y_I = x_A\sin 60° + y_A\cos 60°;\ z_I = \frac{\sqrt{3}}{4}\sin\alpha;$

$x_J = x_F\cos 180° - y_F\sin 180°;\ y_J = x_F\sin 180° + y_F\cos 180°;\ z_J = -\frac{\sqrt{3}}{4}\sin\alpha;$

$x_K = x_A\cos 180° - y_A\sin 180°;\ y_K = x_A\sin 180° + y_A\cos 180°;\ z_K = -\frac{\sqrt{3}}{4}\sin\alpha;$

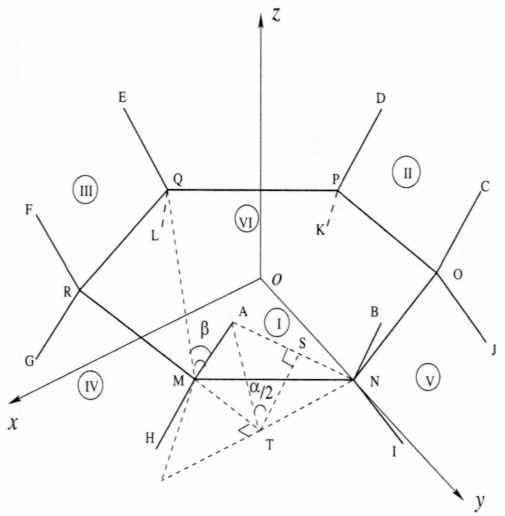

Figure 2.4: Outline of a unit cell with struts and some imaginary lines

$x_L = x_F \cos 300° - y_F \sin 300°$; $y_L = x_F \sin 300° + y_F \cos 300°$; $z_L = -\frac{\sqrt{3}}{4} \sin \alpha$.

We get the coordinates of the above 12 points:

A(1.0104, 0.75, 0.40830), B(0.1443, 1.250, 0.4083), C(-1.1547, 0.50, 0.4083), D(-1.1547, -0.50, 0.4083), E(0.1443, -1.2531, 0.408), F(1.0104, -0.75, 0.4083), G(1.1547, -0.50, -0.4083), H(1.1547, 0.50, -0.4083), I(-0.1443, 1.250, -0.4083), J(-1.0104, 0.75, -0.4083), K(-1.0104, -0.75, -0.4083), L(-0.1443, -1.250, -0.408).

$x_M = \frac{\sqrt{3}}{2}$; $y_M = \frac{1}{2}$; $z_M = 0.0$;

$x_Q = 0$; $y_Q = -1$; $z_Q = 0$.

The vector $\overrightarrow{MA}$ may be represented as:

$\overrightarrow{MA} = [ma_1, ma_2, ma_3] = [x_A - x_M, y_A - y_M, z_A - z_M] = [-\frac{\sqrt{3}}{4} \cos \alpha, \frac{1}{4}, \frac{\sqrt{3}}{4} \sin \alpha]$.

The vector $\overrightarrow{MQ}$ may be represented as:

$\overrightarrow{MQ} = [mq_1, mq_2, mq_3] = [x_Q - x_M, y_A - y_M, z_A - z_M] = [-\frac{\sqrt{3}}{2}, -\frac{3}{2}, 0]$.

Therefore, the angle β between $\overrightarrow{MA}$ and $\overrightarrow{MQ}$ is:

$$\cos \beta = \frac{ma_1 \cdot mq_1 + ma_2 \cdot mq_2 + ma_3 \cdot mq_3}{\sqrt{ma_1^2 + ma_2^2 + ma_3^2} \cdot \sqrt{mq_1^2 + mq_2^2 + mq_3^2}}, \tag{2.2}$$

$\beta = 125.264°$,

$\beta_1 = 180 - \beta = 64.736°$.

2.1.1.3 Calculations of coordinates of eight vertices of the cubic unit cell in the specific axial system

A plane in 3-D space is described as $Ax + By + Cz + D = 0$. All the six planes of the unit cell are represented as following:

Plane I: $A_1x + B_1y + C_1z + 1 = 0$,

which is through points A and B, and is perpendicular to plane II and plane III (to be discussed soon).

Plane II: $A_2x + B_2y + C_2z + 1 = 0$,

which is through points C and D, and is perpendicular to plane I and plane III.

Plane III: $A_3x + B_3y + C_3z + 1 = 0$,

which is through points E and F, and is perpendicular to plane I and plane II.

Plane IV: $A_2x + B_2y + C_2z + D_4 = 0$,

which is through point G and H, and is parallel to plane II.

Plane V: $A_3x + B_3y + C_3z + D_5 = 0$,

which is through point I and J, and is parallel to plane III.

Plane VI: Plane one: $A_1x + B_1y + C_1z + D_6 = 0$,

which is through points K and L, and is parallel to plane I.

Substitute the coordinates of points A, B, C, D, E, F, G, H, I, J, K and L into the foregoing equations and use the geometrical relationships (parallel and perpendicular), we get the coordinates of 8 vertices of the cubic unit cell

(assume the length of an entire strut is 1):

Vertex 1(0, 0, 2.41424), Vertex 2(1.9245, 0, 0.680414), Vertex 3(0.96225, 1.66667, -0.680414), Vertex 4(-0.96225, 1.66667, 0.680414), Vertex 5(-0.96225, -1.66667, 0.680411), Vertex 6(0.96225, -1.66667, -0.680414), Vertex 7(0, 0, -2.041424), Vertex 8(-1.9245, 0, -0.680414).

And the size of the cubic unit cell is 2.589107.

In Figure 2.3, if the length of an entire strut is 1, then the size of the cubic is 2.589107. If we assume that the size of the cubic unit cell is 1, then the length of an entire strut is 0.38623. A Mathematica program is written to obtain these results.

Chapter 3

Unit Cell Meshing

3.1 Geometrical characteristics of the unit cell

3.1.1 Component of the unit cell

The unit cell is very complicated. However, we can further divide it into six U frames. In other words, we can construct six U frames and then assemble them together for getting a unit cell. Figure 3.1 shows the two-dimensional profile of a U frame of the unit cell.

3.1.2 The meshing of a unit cell

To see whether different meshes influence the numerical results significantly, we adopted two meshes different not only in the number of elements but also in the combination of elements. One has 168 elements (60 6-node element and

108 8-node elements), the other has 264 elements (60 6-node elements and 204 8-node elements). Figure 3.1 shows one way to mesh a U frame. Comparisons between the numerical results from the two distinct meshing ways will be done later.

3.2 C++ codes for generating meshes

Constructing meshes is a very important but time consuming step in the finite element analysis. Different meshes could affect the time needed for doing the analysis and sometimes it could determine whether the simulation will be successful or not. For models that are not complicated, manual meshing or using a preprocessing package such as Computer Aided Engineering (CAE) software can be adequate. But the unit cell studied here is a very complicated one, as we need to perform analyses on the unit cells with various void fractions. Therefore, automatic mesh generation using computer programs is necessary to generate meshes very conveniently and efficiently. Most importantly, good design and implementation of codes can make them easily reused in future FEA studies. Three C++ classes were designed and implemented for the generation of the meshes. They are the node class, the element class, and the u_frame class. Their interfaces are described in the following:

```
class node
{
```

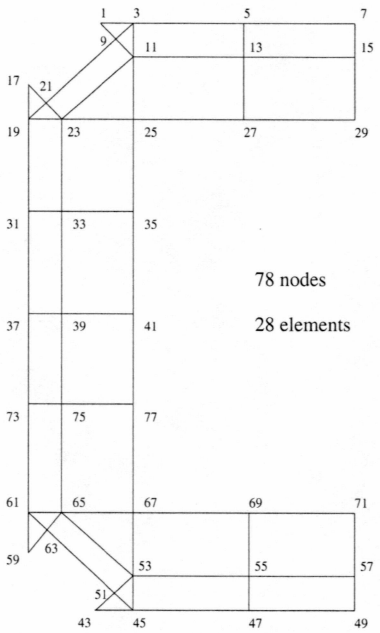

Figure 3.1: A mesh strategy of a U frame

```
 public:
 node( );        //constructor
 node(int n);    //constructor, n is the node number
 void set_number(int n);
 void set_xcoor(float x);
 void set_ycoor(float y);
 void set_zcoor(float z);
 int get_number( );
 float get_xcoor( );
 float get_ycoor( );
 float get_zcoor( );
 private:
 int number;                    //node number
 float xcoor, ycoor, zcoor;     //node coordinates
};
class element
{
  public:
  element( );       //constructor
  element(int n);   //constructor, n is the element number
  set_number(int n);
  set_node(int i, int n);
```

```
  get_number( );
  int get_node(int j);
  private:
  int number;
  int node1, node2, node3, node4, node5, node6, node7, node8;
};
class u_frame
{
  public:
  u_frame( );              //constructor
  u_frame( );              //constructor
  void set_length_size(float l, float s); //set length & size
  int node_number(int i);            //get node number
  float node_coor(int n, int i);     //get node coordinates
  int element_number(int i);      //get the element number
  int element_node(int n, int i); //get element information
  void disp_x(float dx);    //displacement in x direction
  void disp_y(float dy);    //displacement in y direction
  void disp_z(float dz);    //displacement in z direction
  void rotate_x(float rx);  //rotation with respect to x axis
  void rotate_y(float ry);  //rotation with respect to y axis
  void rotate_z(float tz);  //rotation with respect to z axis
```

```
    private:
    float length;    //length of an entire strut
    float size:      //size of the cross section of the struts
    node u_node[NODENUMBER];
    element u_element[ELEMENTNUMBER];
    void calculate_coor( ); //calculate coordinate of nodes
    void build_elements( ); //build elements usingusing nodes
};
```

A whole unit cell consists of six U frames. We need to put six meshed U frames together to get the mesh of an entire unit cell. Therefore, extra work must be done such as rearranging all the node and element numbers and deleting redundant nodes. A few functions are designed to deal with these problems to accomplish the following tasks:

1. Make the node number continuous;
2. Get rid of the redundant nodes;
3. Update the element information based on the above node changes;
4. Set the boundary for the unit cell.

Figure 3.2 is the flow chart for generating FEA meshes used by ABAQUS.

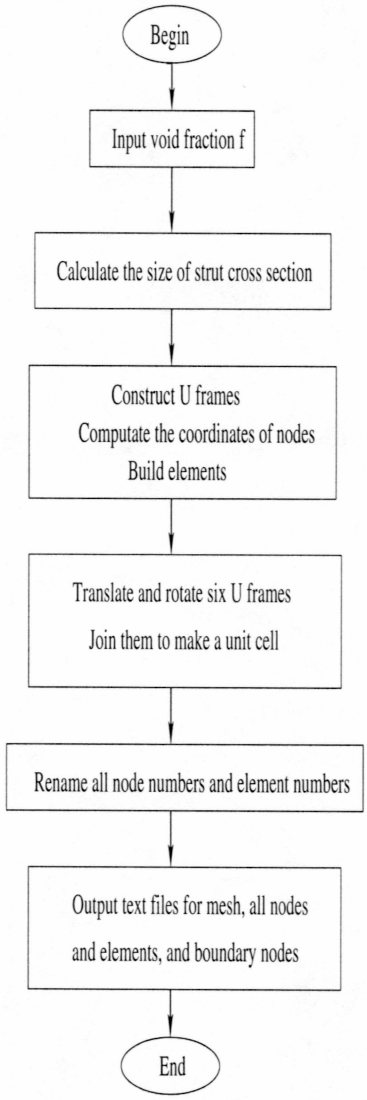

Figure 3.2: Flow chart of mesh construction

3.3 Unit cell meshes generated by C++ codes

Figure 3.3 to Figure 3.10 are the meshes generated by the C++ programs for the unit cells with $f = 0.55$, $f = 0.60$, $f = 0.65$, $f = 0.70$, $f = 0.75$, $f = 0.80$, $f = 0.84$, and $f = 0.90$, respectively, each with 168 elements. Figure 3.11 to Figure 3.13 show another version of meshes generated for the unit cells with $f = 0.80$, $f = 0.84$, and $f = 0.90$, each with 264 elements.

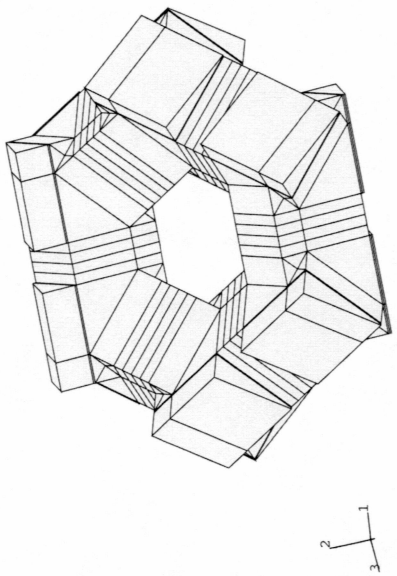

Figure 3.3: The mesh of the unit cell with $f = 0.55$ and 168 elements

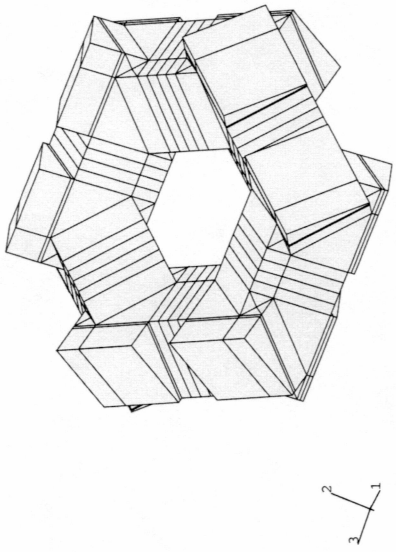

Figure 3.4: The mesh of the unit cell with $f = 0.60$ and 168 elements

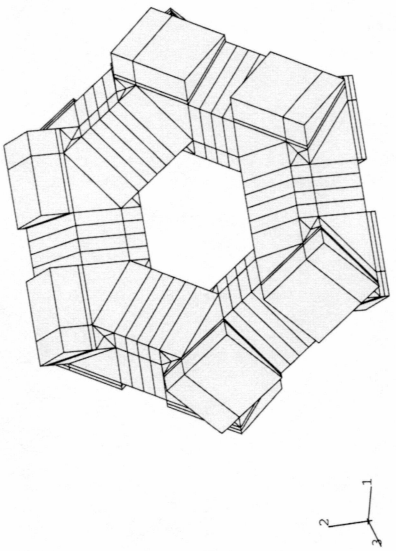

Figure 3.5: The mesh of the unit cell with $f = 0.65$ and 168 elements

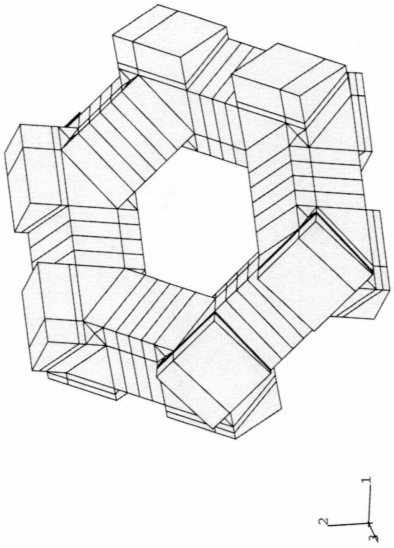

Figure 3.6: The mesh of the unit cell with $f = 0.70$ and 168 elements

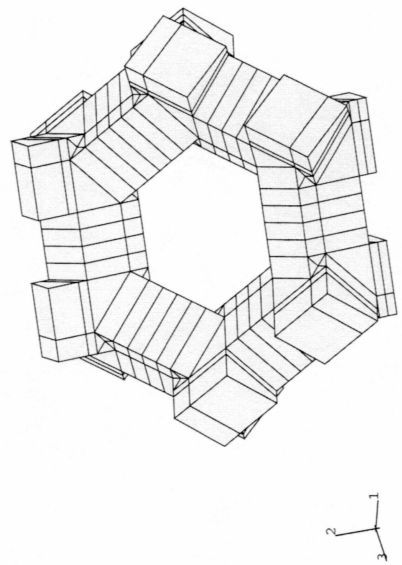

Figure 3.7: The mesh of the unit cell with $f = 0.75$ and 168 elements

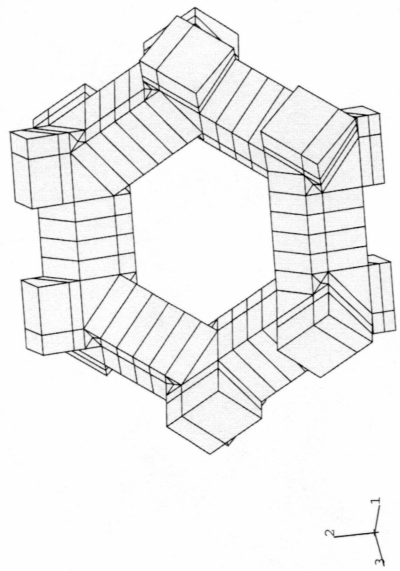

Figure 3.8: The mesh of the unit cell with $f = 0.80$ and 168 elements

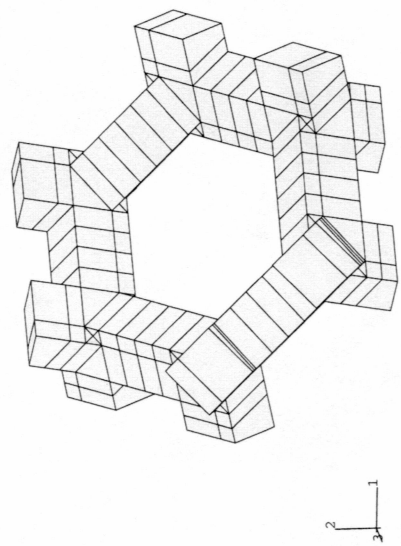

Figure 3.9: The mesh of the unit cell with $f = 0.84$ and 168 elements

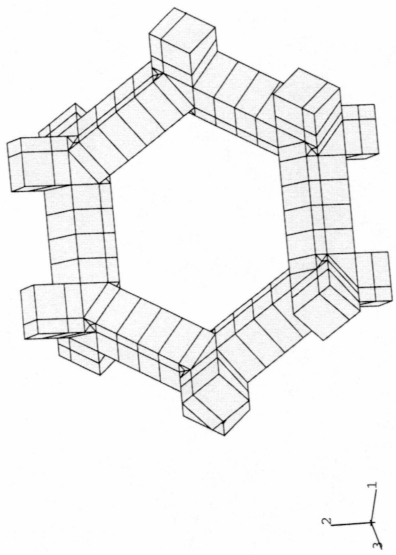

Figure 3.10: The mesh of the unit cell with $f = 0.90$ and 168 elements

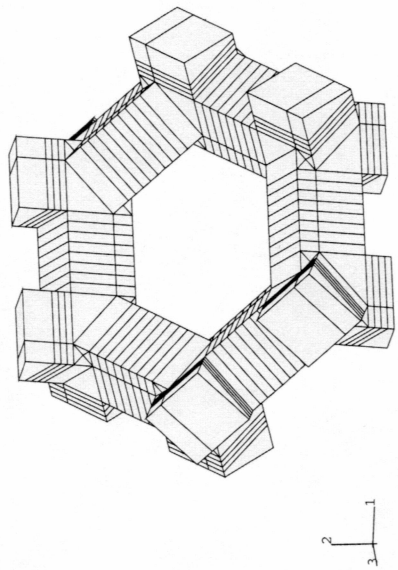

Figure 3.11: The mesh of the unit cell with $f = 0.80$ and 264 elements

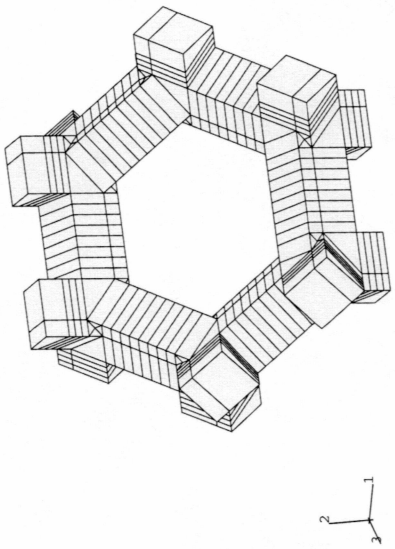

Figure 3.12: The mesh of the unit cell with $f = 0.84$ and 264 elements

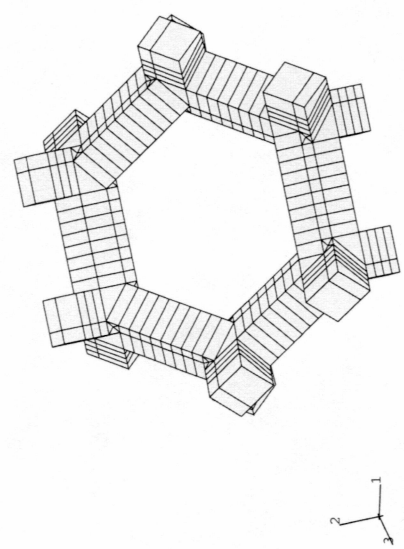

Figure 3.13: The mesh of the unit cell with $f = 0.90$ and 264 elements

Chapter 4

Numerical Solutions

4.1 Boundary conditions and material properties

4.1.1 Material properties

In the studies of the unit cell, the fundamental material properties needed are those of the solid material (the matrix) that make up the porous materials. Although the macroscopic properties of the porous materials could be measured, there are very little data in open literature for the matrix material properties. In this study, the Young's modulus of the solid material (polyurethane) is estimated to be 22,777.8 *psi* and the yield strength (σ_0) is estimated to be 1,500 *psi* (Table 2, Triantafillou et al., 1989).

Table 4.1: Eight boundary conditions (displace controls)

Case	D_x	D_y	D_z	$D_x : D_y : D_z$
1	0.00	0.00	0.30	0.00 : 0.00 : 1.00
2	0.08	0.08	0.08	1.00 : 1.00 : 1.00
3	0.42	0.00	-0.42	1.00 : 0.00 : -1.00
4	0.04	0.07	0.08	1.00 : 1.75 : 2.00
5	-0.08	0.00	0.308	-1.00 : 0.00 : 3.85
6	0.30	0.00	-0.20	1.00 : 0.00 : 0.667
7	0.075	0.12	0.03	1.00 : 1.60 : 0.40
8	0.04	0.16	0.02	1.00 : 4.00 : 0.500

4.1.2 Loads applied on the unit cell

Two types of boundary loads, stress and displacement, can be applied on the models. Under stress control, the stress is applied gradually until yielding occurs in the model. Under displacement control, the displacement is applied gradually until yielding takes place in the model. The disadvantage of the stress control is that the shape of the unit cell can not be maintained when a uniformly distributed stress is applied to it. In our studies, we need to know the deformation of the unit cell and two different kinds of stress versus strain curves for the analysis. Therefore, in order to better simulate the deformation of the unit cells in the foam, the displacement control is taken in the numerical simulation. Table 4.1 shows the loads for eight various cases used in our studies. D_x is the displacement in the x direction, D_y is the displacement in the y direction, D_z is the displacement in the z direction.

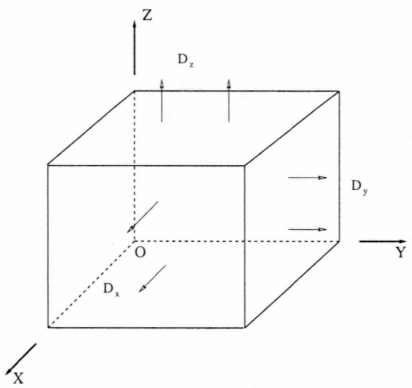

Figure 4.1: The boundary conditions of the unit cell

4.1.3 Constraints

The constraints used are as follows. The top, right and front surfaces of the unit cell have displacement loading. The other three surfaces of the unit cell are constrainted to be flat by rollers. This preserves the shapes of these faces but allows deformations to occur while taking into consideration the effect of the interaction of the neighboring unit cells. Figure 4.1 shows the outline of the unit cell and boundary conditions. For simplicity, solid struts are ignored.

4.2 An ABAQUS input file

The ABAQUS input data file is a text file which provides information necessary to perform the finite element analysis. It mainly includes node sets, node subsets, element sets, element subsets, element types, material properties, boundary conditions and constraints, and processing and output information control commands. The following is an example of an input data file (kelvin.inp for one case) used in our finite element analyses. Six node sets which include xpositive, xnegative, ypositve, ynegative, zpositive, znegative are for the nodes on the six surfaces of the unit cell, respectively.

```
*HEADING
perfect plastic analysis for open cell Kelvin foams
*RESTART, WRITE, FREQ=1
*NODE
9991, 2.0, 2.0, 2.0
*NODE, NSET=TOP, INPUT=zpositive
*NODE, NSET=BOT, INPUT=znegative
*NODE, NSET=RIGHT, INPUT=ypositive
*NODE, NSET=LEFT, INPUT=ynegative
*NODE, NSET=FRONT, INPUT=xpositive
*NODE, NSET=REAR, INPUT=xnegative
*NODE, NSET=NALL, INPUT=nodes
*ELEMENT, TYPE=C3D8, ELSET=FOAM8, INPUT=ele8ment
```

```
*ELEMENT, TYPE=C3D6, ELSET=FOAM6, INPUT=ele6ment
*ELSET, ELSET=FOAM
FOAM8, FOAM6
*SOLID SECTION, ELSET=FOAM, MATERIAL=EL
*MATERIAL, NAME=EL
*ELASTIC, TYPE=ISOTROPIC
22777.8, 0.3
*PLASTIC
1500.0, 0.0
*BOUNDARY
REAR, 1
LEFT, 2
BOT, 3
*EQUATION
2
FRONT, 1, 1.0, 9991, 1, -1.0
2
RIGHT, 2, 1.0, 9991, 2, -1.0
2
TOP, 3, 1.0, 9991, 3, -1.0
*STEP, INC=1000, NLGEOM
*STATIC
```

```
0.08, 2.0, , 0.1
*BOUNDARY
** case 2
9991, 3, , 0.08
9991, 1, , 0.08
9991, 2, , 0.08
*EL PRINT
S, MISES
E
PE
*NODE PRINT
U
RF
*NODE FILE
U, COORD
RF
*END STEP
```

4.3 Numerical results

4.3.1 Loading path

By definition, a macroscopic normal stress can be expressed in terms of the reaction force,

$$\Sigma_i = \frac{F_i}{A_i}, \tag{4.1}$$

where Σ_i is the macroscopic stress; A_i is the area of the surface in a certain direction, and $i = 1, 2, 3$; F_i is the reaction force on surface A_i which can be extracted from the ABAQUS output file (*.fil) through ABAQUS interfaces. The macroscopic shear stresses are zero in our finite element models because of the constraints we used. It is easy to calculate the macroscopic equivalent stress (Σ_{equ}) and the mean stress (Σ_m),

$$\Sigma_{equ} = \sqrt{\frac{1}{2}[(\Sigma_1 - \Sigma_2)^2 + (\Sigma_2 - \Sigma_3)^2 + (\Sigma_3 - \Sigma_1)^2]}, \tag{4.2}$$

$$\Sigma_m = \frac{1}{3}(\Sigma_1 + \Sigma_2 + \Sigma_3). \tag{4.3}$$

The following is a Fortran code used for getting the mean and equivalent stresses.

```
C  LOADING TRACK IN MACRO-STRESSES FOR KELVIN OPEN CELL FOAMS
```

```
      PROGRAM PERT
      IMPLICIT REAL*8 (A-H,O-Z)
      CHARACTER*80 FNAME
      CHARACTER*80 OUTFILE
      DIMENSION ARRAY(513), JRRAY(513), RB(5,41), LRUNIT(2,1)
      DIMENSION DISPX(200),DISPY(200),DISPZ(200)
      EQUIVALENCE (ARRAY(1), JRRAY(1))
C  FILE INITIALIZATION
      WRITE(*,*) 'INPUT FILE NAME(jobname):'
      READ(*,*) FNAME
      WRITE(*,*) 'OUTPUT FILE NAME(jobname):'
      READ(*,*) OUTFILE
      WRITE(*,*) 'WAITING...'
C  READ VALUES FROM FILE OUTPUT ON UNIT 8
C  WRITE RESULT TO UNIT 6
      OPEN(6,FILE=OUTFILE)
      NRU=1
      LRUNIT(1,1)=8
      LRUNIT(2,1)=2
      LOUTF=1
      CALL INITPF(FNAME,NRU,LRUNIT,LOUTF)
      JUNIT=8
```

```
      CALL DBRNU(JUNIT)
C  LOOP ON ALL RECORDS IN RESULTS FILE
      TT=1500.0                !strut yield strength
      DO 100 K1=1,9999999
      CALL DBFILE(0,ARRAY,JRCD)
      IF(JRCD .NE. 0) GO TO 110
      KEY=JRRAY(2)
C  GET REACTION FORCE FROM .fil
      IF(KEY.EQ.104) THEN
        NODE=JRRAY(3)
        IF(NODE.EQ.9991) THEN
          F1=ARRAY(4)
          F2=ARRAY(5)
          F3=ARRAY(6)
C  CALCULATION AND OUTPUT
          WRITE(*,*) F1,F2,F3
          SM=(F1+F2+F3)/3/TT
          SP1=F1/TT-SM
          SP2=F2/TT-SM
          SP3=F3/TT-SM
          SEQ=SQRT(3/2*(SP1*SP1+SP2*SP2+SP3*SP3))
          WRITE(6,120) SM,SEQ
```

```
          END IF
        END IF
100     CONTINUE
110     CONTINUE
        CLOSE(6)
120     FORMAT(5X,5X,2E15.6)
        STOP
        END
```

The simulation results of the FEA can be presented by the macroscopic stresses: Σ_{equ} versus Σ_m representing loading path or loading curve. Figure 4.2 is the loading path for the unit cell with $f = 0.84$ and $D_x : D_y : D_z = 1.00 : 4.00 : 0.50$. It should be noted that the macroscopic stresses are normalized by the yield strength of the wall material. At first the curve follows a straight line while stresses are increasing. Then, beginning at a critical point (point P_y in Figure 4.2), the loading path deviates from the straight line and changes direction significantly. In other words, from a macroscopic point of view, the loading path is composed of elastic and plastic parts and the point at which the loading path deviates is called the transition point.

4.3.2 Equivalent stress versus equivalent strain curve

The equivalent strain can be calculated as

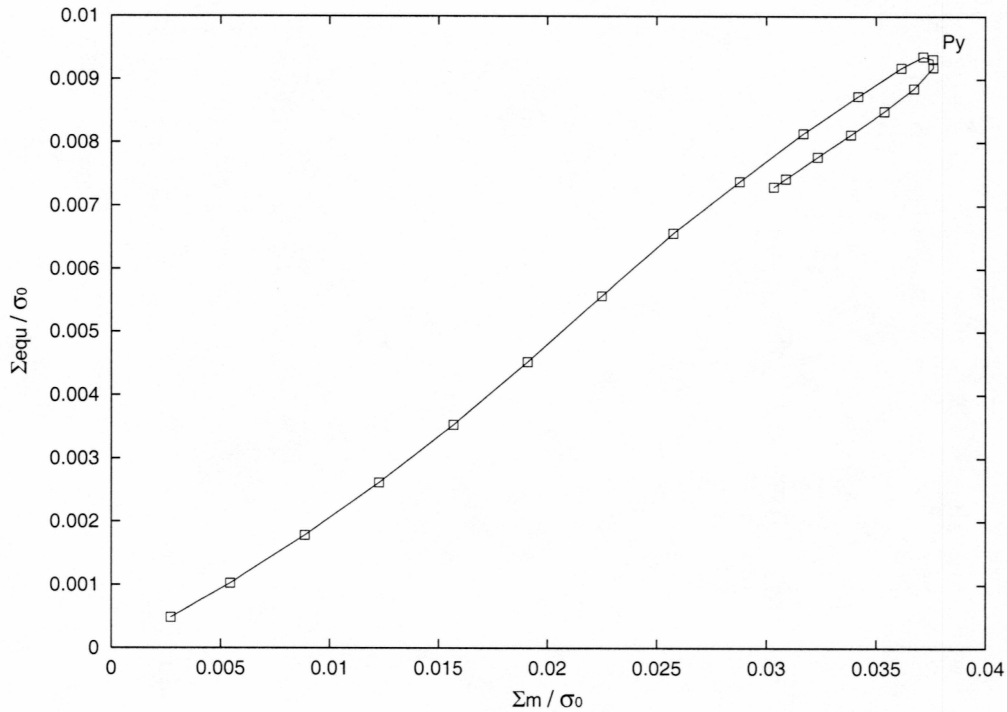

Figure 4.2: The loading path for the unit cell with $f = 0.84$ under loading case 8

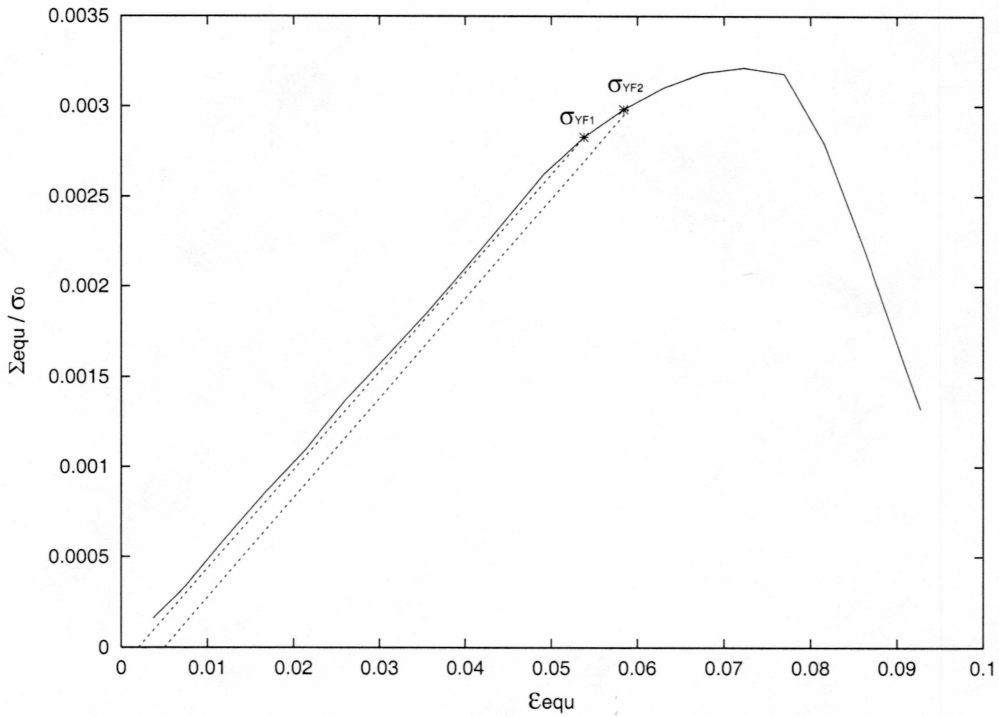

Figure 4.3: The tensile response of the unit cell with $f = 0.84$, case 4, σ_{YF1} is the yield point by using $\varepsilon_p = 0.2\%\,(plastic\,strain)$, σ_{YF2} is the yield point by using $\varepsilon_p = 0.5\%$

$$\varepsilon_{equ} = \sqrt{\frac{2}{3}\varepsilon_{ij}\varepsilon_{ij}}, \tag{4.4}$$

where $\varepsilon_{ij} = \frac{\triangle l_{ij}}{l}$; l is the initial size of the unit cell; $\triangle l_{ij}$ is the change in l.

For each FEA case, displacements of all nodes for every increment are recorded to find ε_{ij}. Figure 4.3 is the equivalent stress versus equivalent strain curve acquired from FEA results for the unit cell with $f = 0.84$, case 4 (D_x : D_y : $D_z = 1.00 : 1.75 : 2.00$). The vertical axis is normalized using σ_0, the yield strength of the wall material of the foam (1,500 psi).

4.3.3 Mean stress versus mean strain curve

It is well-known that for hydrostatic loading, the equivalent stress versus equivalent strain curve is not availabe because the equivalent stress is alway equal to zero. In order to get the yield points of the foams under hydrostatic load cases, we use the mean stress versus mean stain curve. The mean strain is defined as

$$\varepsilon_m = \frac{\varepsilon_{11} + \varepsilon_{22} + \varepsilon_{33}}{3}, \tag{4.5}$$

where ε_{ii} $(i = 1, 2, 3)$ is defined as the previous section.

Figure 4.4 is a mean stress versus mean strain curve for the unit cell with $f = 0.84$.

4.3.4 Yield points

There are a few ways to decide the yield point of the foam: the transition point method on the loading path curve (Oung, 1999), back extrapolation (Deshpande, 2001), and 0.2% ε_p method for uniaxial tests on solid materials. The transition point method overestimates the yield strength. It tells the point that most of the entire unit cell fails, not the initial yield point. Back extrapolation has been used in experiments (Deshpande, 2001). It needs to know the fracture point of the material test, so is not good for non-metallic foams. In this thesis, we mainly use the 0.2% ε_p method to get the yield points for getting yield surfaces. In addition, in order to understand the behavior of different methods in

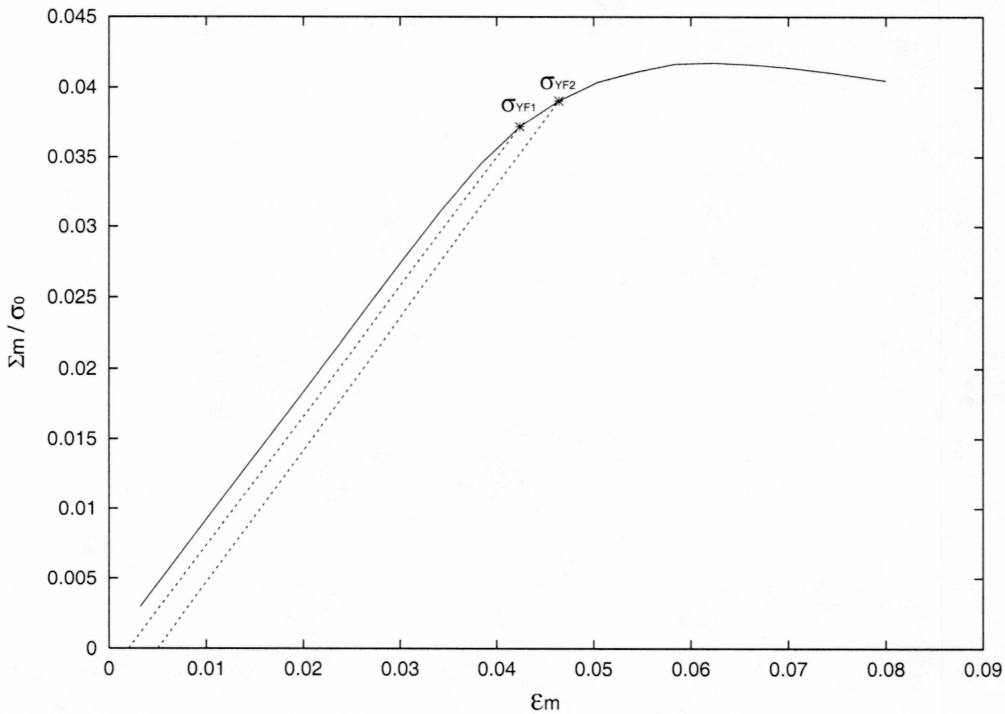

Figure 4.4: The tensile response of the unit cell with $f = 0.84$ under hydrostatic load case. σ_{YF1} is the yield point by using $\varepsilon_p = 0.2\%$, σ_{YF2} is the yield point by using $\varepsilon_p = 0.5\%$

finding the yield surfaces, we employed the transition point method (shown in Figure 4.2) for the unit cell with $f = 0.84$, 0.2% ε_p method and 0.5% ε_p method (in Figure 4.3 and Figure 4.4) on two foams with $f = 0.84$ and $f = 0.92$. The yield point in Figure 4.2 is the point at which the foam starts to be at failure. The yield points in Figure 4.3 and Figure 4.4 are the initial yield points of the foam. Figure 4.5 shows two groups of yield points for the unit cell with $f = 0.84$ from 0.2% ε_p method and 0.5% ε_p method. According to this figure, we see that they are very close except some difference on a couple of points near the axis of the normalized mean stress. Therefore in this thesis, only one of these two methods (0.2% ε_p method) is mainly chosen for taking yield points. More details of difference in results from these three methods will be discussed later.

4.3.5 Yield surfaces

For a unit cell with a certain void fraction f, by applying different ratios of external loads, displacements or forces ($D_x : D_y : D_z$) on it, we can get a series of loading paths. There is a yield point for each loading path. By connecting all the yield points, we can get a curve called the yield surface: a surface in stress-space describing the combination of stresses which cause yield failure. Figure 4.6 shows the FEA yield surface for the unit cell with $f = 0.55$ using the 0.2% ε_p method. The yield surfaces of other models can also be determined by using the same method. Figure 4.7 to Figure 4.13 show the FEA results from other

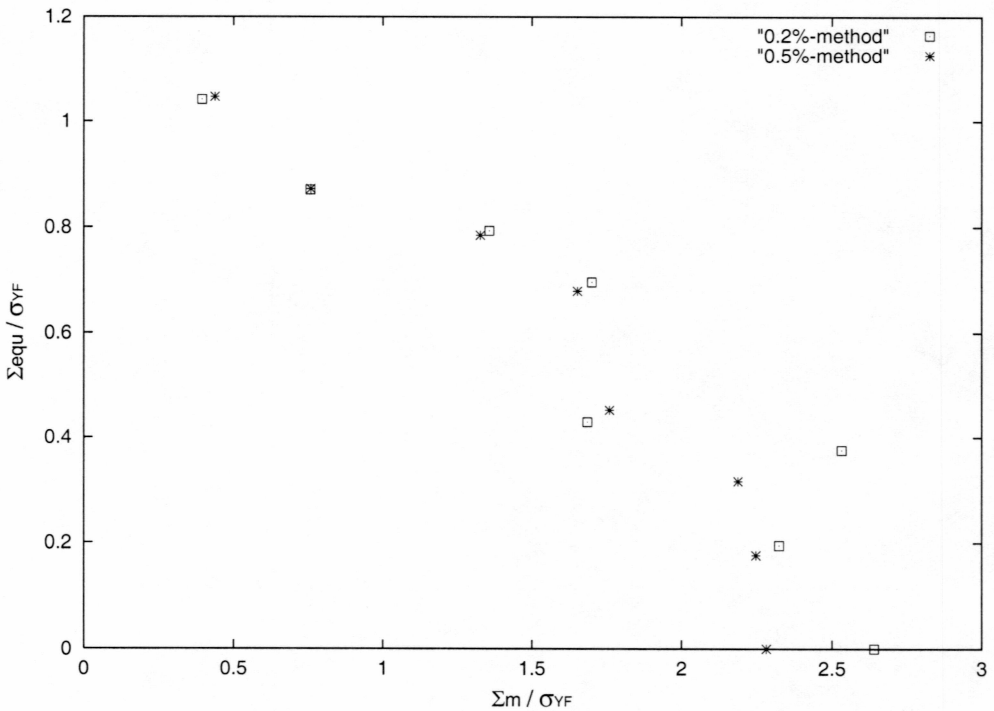

Figure 4.5: Two kinds of yield results for the unit cell with $f = 0.84$ from 0.2% ε_p method and 0.5% ε_p method. σ_{YF} is the uniaxial tensile yield strength of the foams

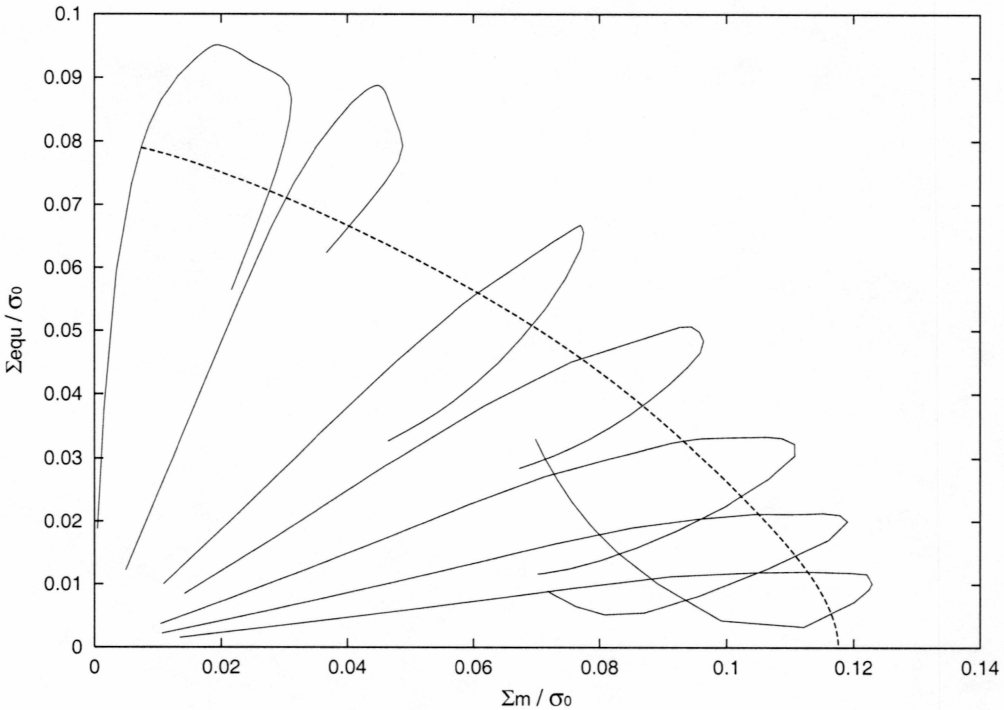

Figure 4.6: The FEA yield surface for the unit cell with $f = 0.55$

unit cells with void fractions $f = 0.60, 0.65, 0.70, 0.75, 0.80, 0.84, 0.92$.

4.3.6 Comparisons between results from different meshes of a unit cell

It is well known that meshing is a very important step in finite element analysis. It not only takes the large part of time for an entire numerical simulation, but also determines whether the FEA will be successful or not. A good mesh may greatly facilitate the whole analysis. There are different ways to mesh a model (unit cell), some are good, some bad. For good meshes, FEA results should

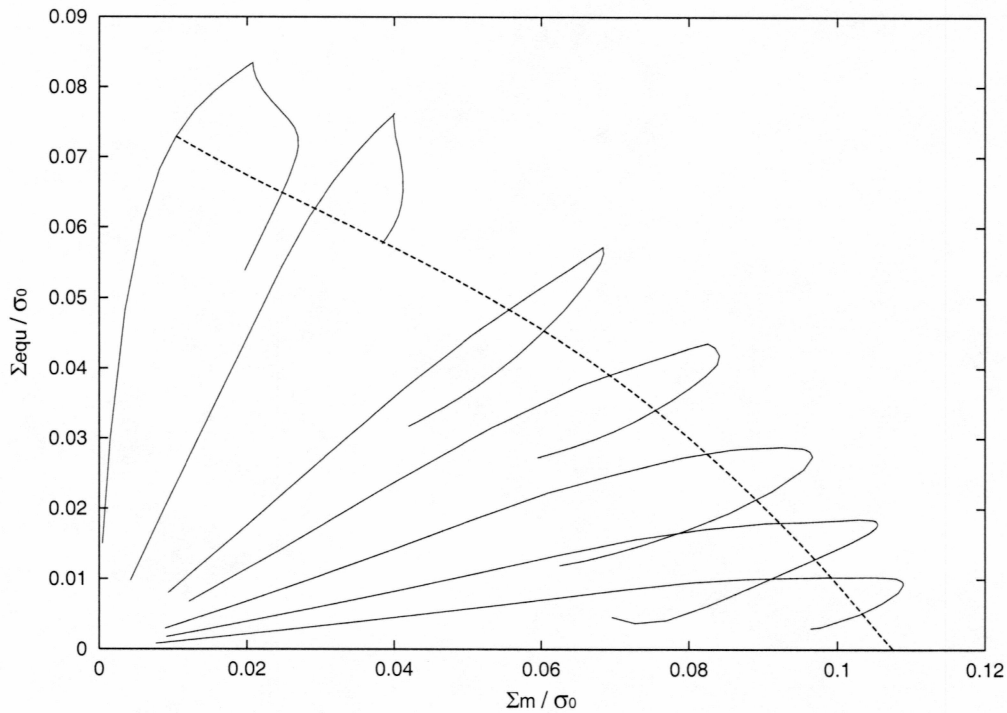

Figure 4.7: The FEA yield surface for the unit cell with $f = 0.60$

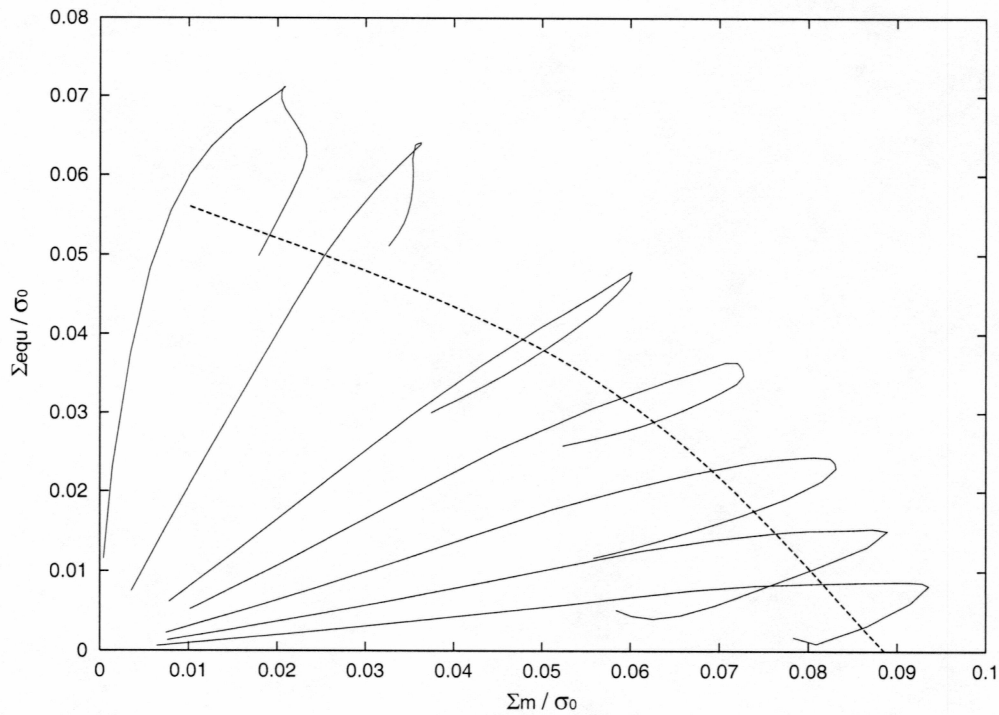

Figure 4.8: The FEA yield surface for the unit cell with $f = 0.65$

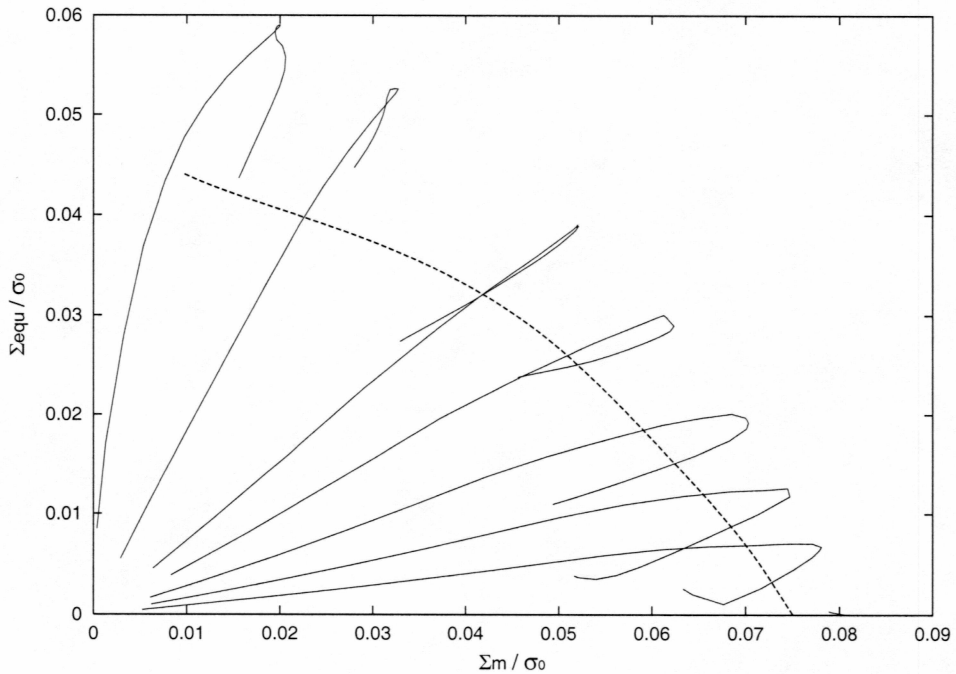

Figure 4.9: The FEA yield surface for the unit cell with $f = 0.70$

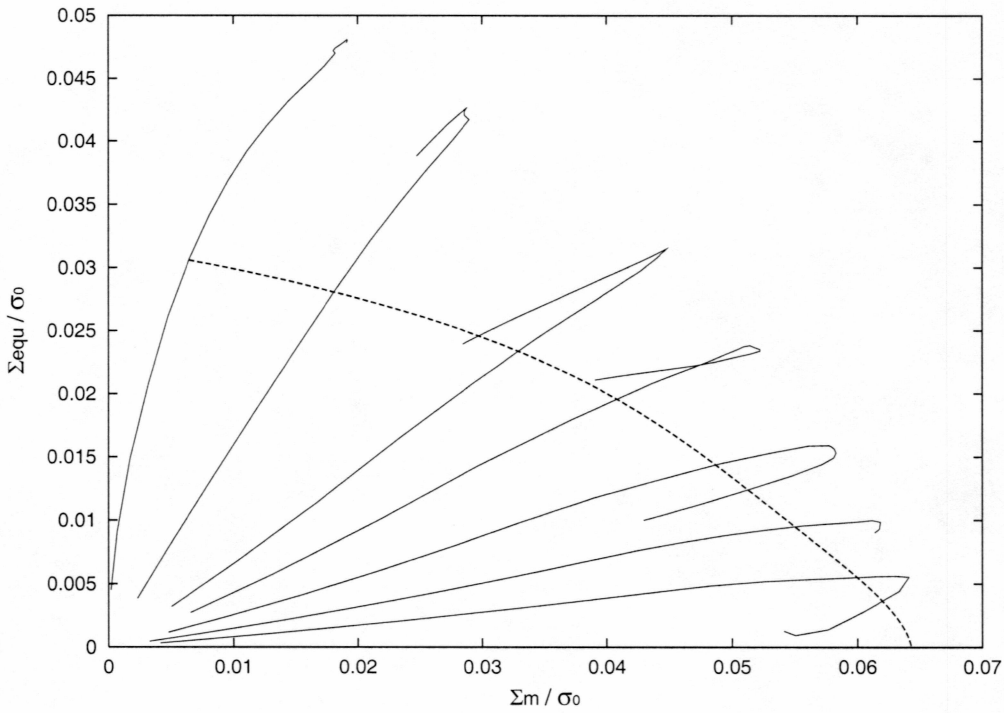

Figure 4.10: The FEA yield surface for the unit cell with $f = 0.75$

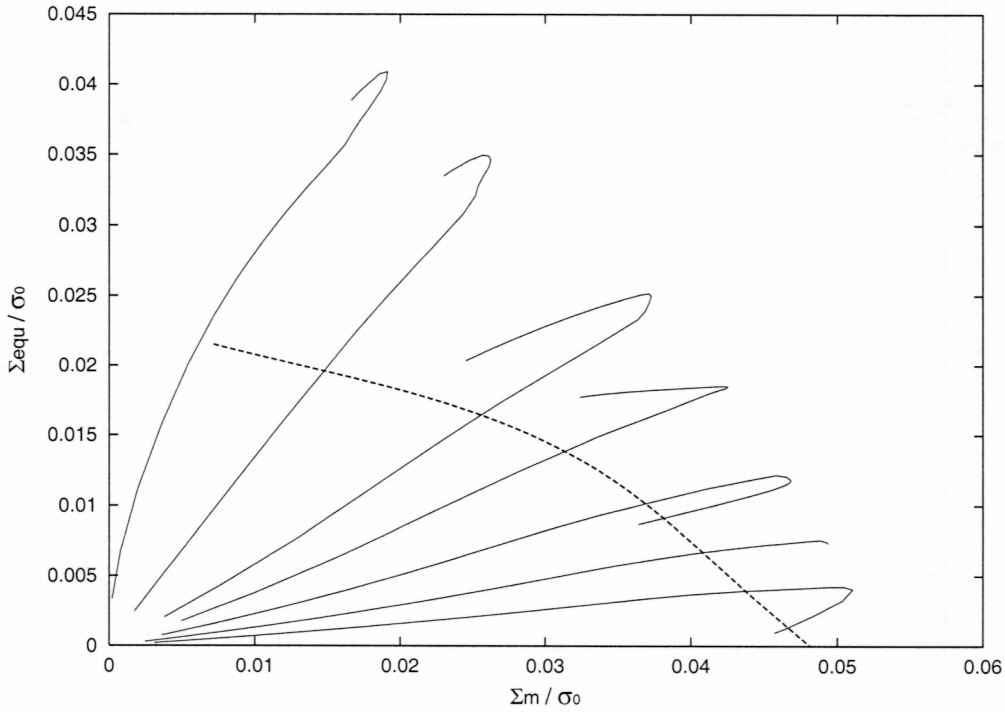

Figure 4.11: The FEA yield surface for the unit cell with $f = 0.80$

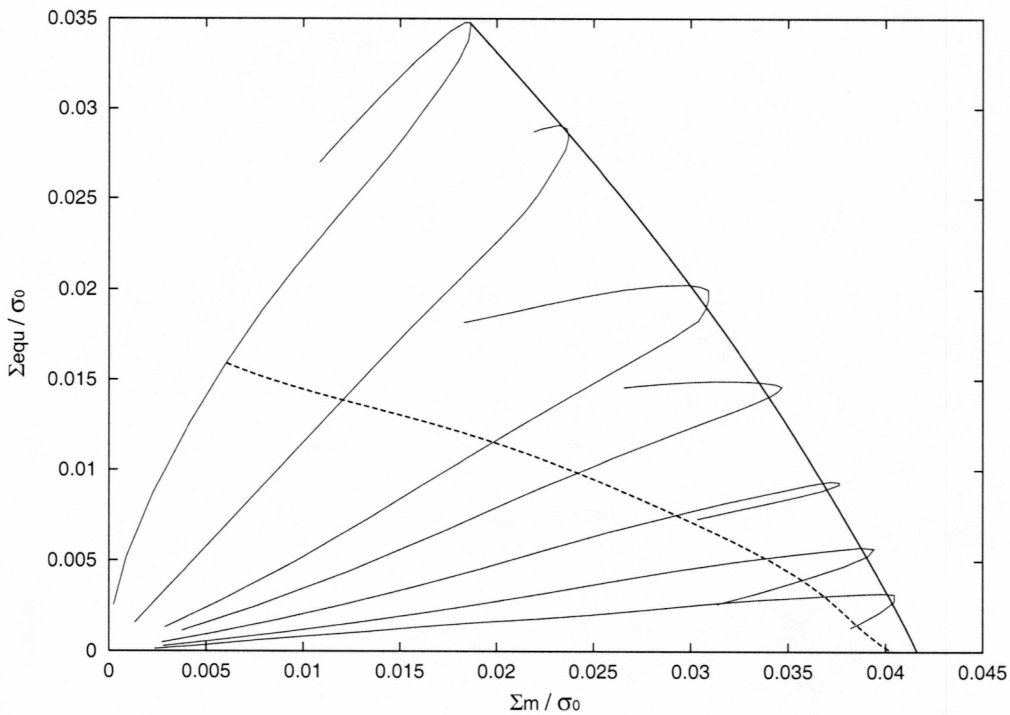

Figure 4.12: Two FEA yield surfaces for the unit cell with $f = 0.84$, dotted – obtained by using the 0.2% ε_p method; thick solid – obtained by using the transition point method

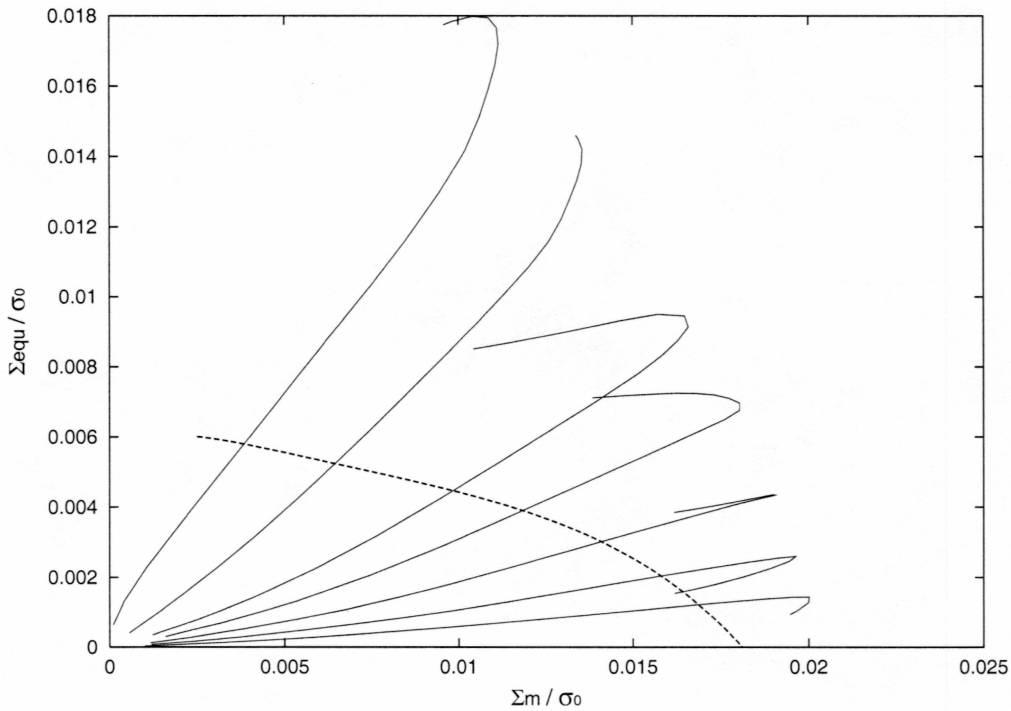

Figure 4.13: The FEA yield surface for the unit cell with $f = 0.92$

Table 4.2: The details of two kinds of meshes for the unit cell

Mesh	Total Nodes	Total Elements	C3D8 Element	C3D6 Element
1	432	168	108	60
2	720	264	204	60

show good consistency for the same FEA case. To make sure the FEA results are accurate, two types of meshes for the unit cells were used for the simulations. Table 4.2 shows the details of these two kinds of meshes. C3D8 element and C3D6 element in ABAQUS are used here. C3D6 element is a 6-node linear triangular prism, C3D8 is an 8-node linear brick. Figure 4.14 and Figure 4.15 show the FEA results from two different meshes for the unit cells with $f = 0.80$ and $f = 0.90$ with nearly identical results. Therefore, the two meshes we used are practical for the unit cells.

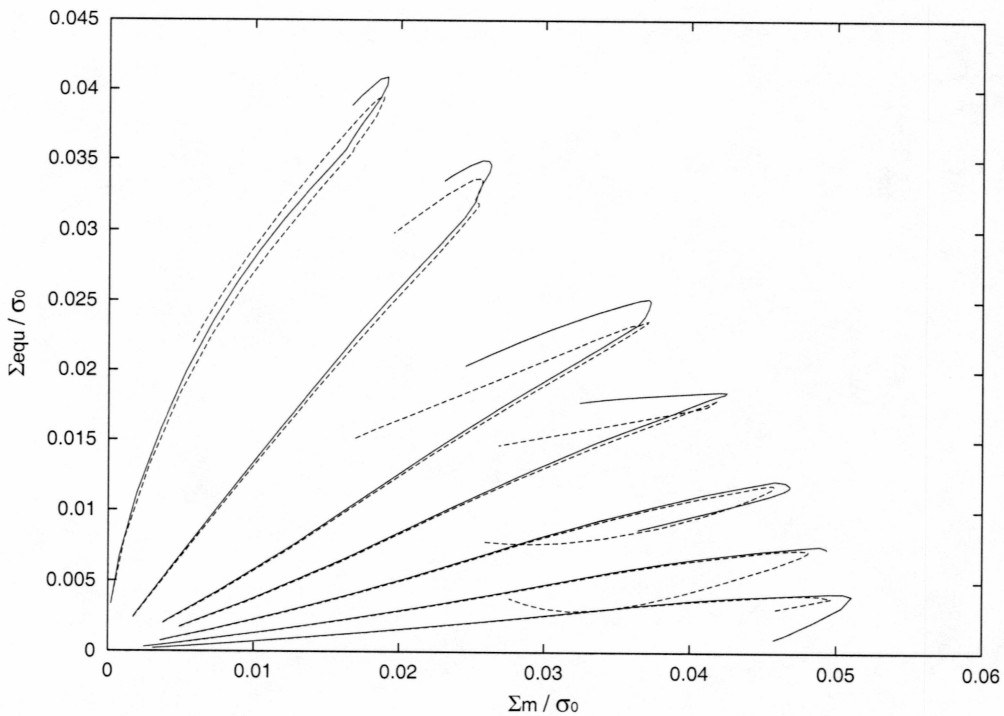

Figure 4.14: FEA loading paths from two different meshes for the unit cell with $f = 0.80$, solid – mesh 1 with 168 elements; dotted – mesh 2 with 264 elements

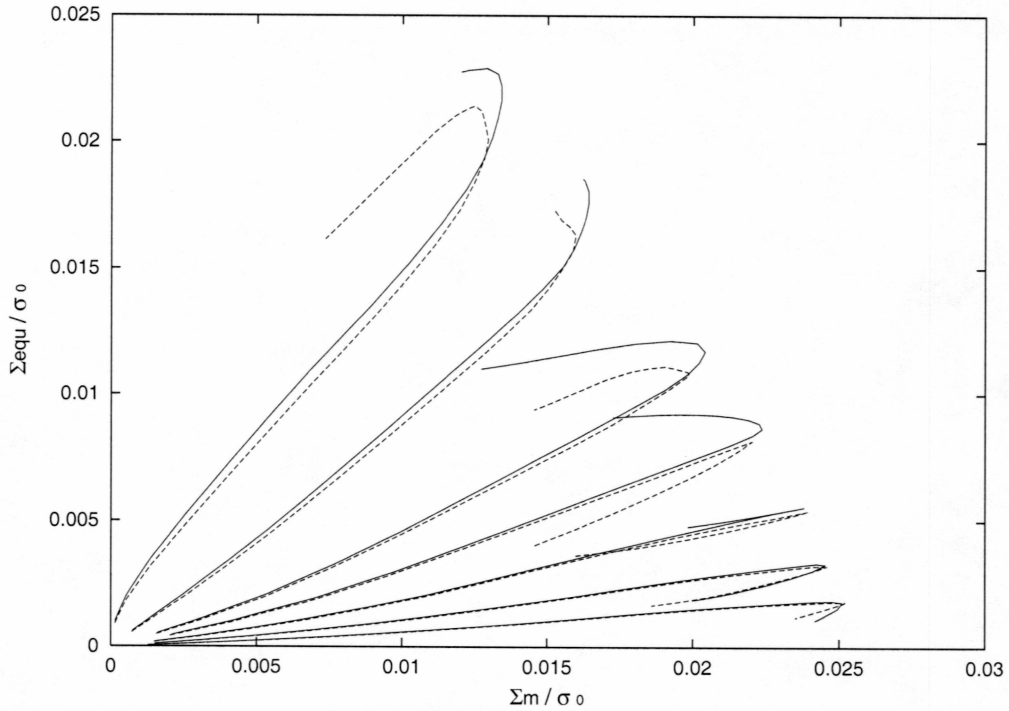

Figure 4.15: FEA loading paths from two different meshes for the unit cell with $f = 0.90$, solid – mesh 1 with 168 elements; dotted – mesh 2 with 264 elements

Chapter 5

Comparisons between existing analytical models, experimental data and numerical models

5.1 Analytical models

Gibson et al. (1989) modeled the the elastic buckling, plastic yield and brittle fracture of cellular solids under multiaxial stresses to develop equations describing their yield surfaces. A yield function was approximately obtained by analyzing the development of the plastic hinges in the honeycomb (2-D cell) first and then extended to the 3-D frame (foams). The yield function was then truncated by a fast brittle fracture criterion in the tension side and an elastic buckling limit criterion in the compression side to form a failure criterion of the

foams.

$$\frac{\sigma_d}{\sigma_{ys}} = \pm\gamma \left(\frac{\rho^*}{\rho_s}\right)^{3/2} \left\{1 - \left[\frac{3\sigma_m}{\sigma_{ys}\left(\rho^*/\rho_s\right)}\right]^2\right\}. \tag{5.1}$$

The constant γ is obtained as:

$$\gamma\left[1 - 0.009\left(\rho^*/\rho_s\right)\right] = 0.3. \tag{5.2}$$

For all interested values of ρ^*/ρ_s (less than about 0.3), $\gamma \approx 0.3$. The yield criterion for foams under multiaxial stresses is:

$$\frac{\sigma_d}{\sigma_{ys}} = \pm 0.3 \left(\frac{\rho^*}{\rho_s}\right)^{3/2} \left\{1 - \left[\frac{3\sigma_m}{\sigma_{ys(\rho^*/\rho_s)}}\right]^2\right\}, \tag{5.3}$$

where σ_d is the equivalent stress, σ_{ys} is the yield stress of the solid cell wall material, ρ^* is the density of the bulk material, σ_s is the density of the solid cell wall material, σ_m is the mean stress. In terms of void fraction f, the normalized equivalent stress $\frac{\Sigma_{equ}}{\sigma_0}$ and the normalized mean stress $\frac{\Sigma_m}{\sigma_0}$ (σ_0 is the yield strength of the wall material), the above equation can be described as following:

$$\frac{\Sigma_{equ}}{\sigma_0} = \pm 0.3\left(1 - f\right)^{3/2} \left\{1 - \left[\frac{3\Sigma_m}{\sigma_0\left(1 - f\right)}\right]^2\right\}. \tag{5.4}$$

Lee and Zhang (2002) studied the plastic behavior of foams with an open-celled structure. They developed an approximate continuum plasticity model within the framework of the upper bound theorem of plasticity to describe the

yield behavior of foams, and derived the microscopic velocity field for the unit cell, which satisfies the incompressibility and the kinematic boundary conditions. From the microscopic velocity fields, a macroscopic yield function is developed for foams under multiaxial stresses and includes the effects of the hydrostatic stress due to the presence of void and its grow,

$$\Phi = \left(\frac{\Sigma_{equ}}{\sigma_0}\right)^2 - \frac{92}{3 \times 456^2}\left(74 - 123f + 49f^2\right) \tag{5.5}$$

$$\left[1 - \frac{456^2 \Sigma_M^2}{46\sigma_0^2\left(\frac{441}{4} - \frac{741}{4}f + 75f^2\right)}\right], \tag{5.6}$$

where f is the void fraction.

5.2 Comparisons of yield surfaces

Figure 5.1 to Figure 5.8 show FEA yield surfaces and analytical ones for unit cells with void fraction $f = 0.65, 0.70, 0.75, 0.80, 0.84, 0.92$. In Figure 5.6 and Figure 5.7, the FEA yield surfaces are acquired by the 0.5% ε_p method and the transition point method, respectively. Note that we normalized the equivalent stress and mean stress by using the uniaxial yield tensile strength of the foam (σ_{YF}). σ_{YF} can be taken from the FEA yield surfaces in which the equivalent stress and mean stress are normalized by the yield strength of the wall material. It is the intersection of the yield surface and the line with a slope of 3. It is because that for the uniaxial load test, the equivalent stress is three times that

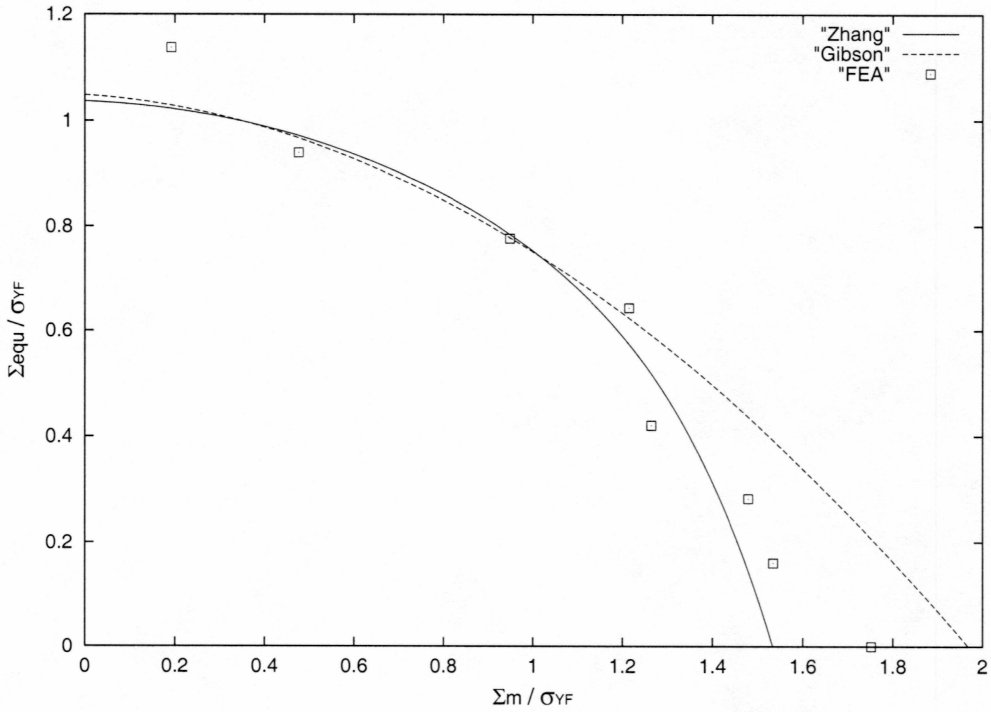

Figure 5.1: Yield surfaces for the unit cell with $f = 0.65$, the FEA surface obtained by using the 0.2% ε_p method

of the mean stress, $\sigma_{equ} = 3\sigma_m$.

Two ways are used to get yield surfaces for the unit cell with $f = 0.84$. It shows that the yield surface by using the 0.2% ε_p method is closer to Gibson's. So mainly we use this method in this thesis.

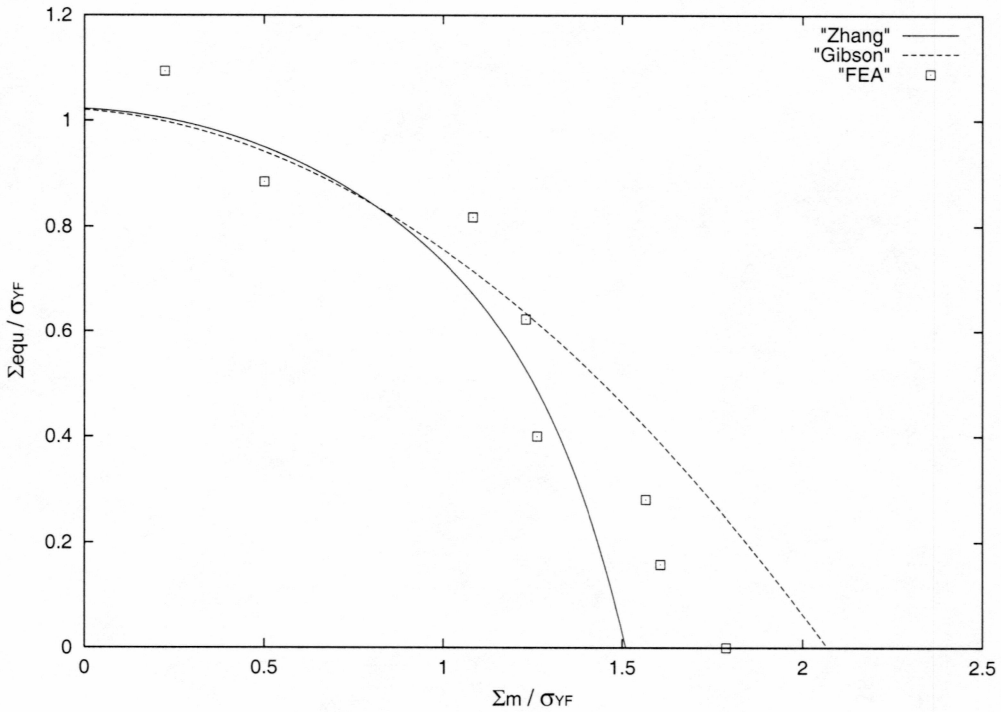

Figure 5.2: Yield surfaces for the unit cell with $f = 0.70$, the FEA surface obtained by using the 0.2% ε_p method

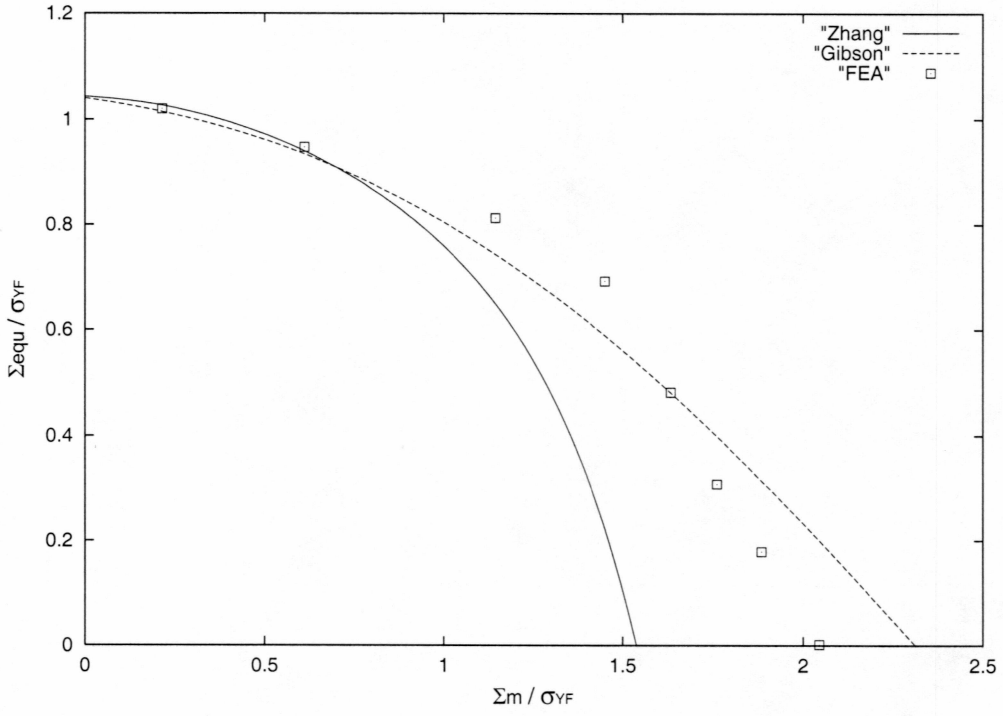

Figure 5.3: Yield surfaces for the unit cell with $f = 0.75$, the FEA surface obtained by using the 0.2% ε_p method

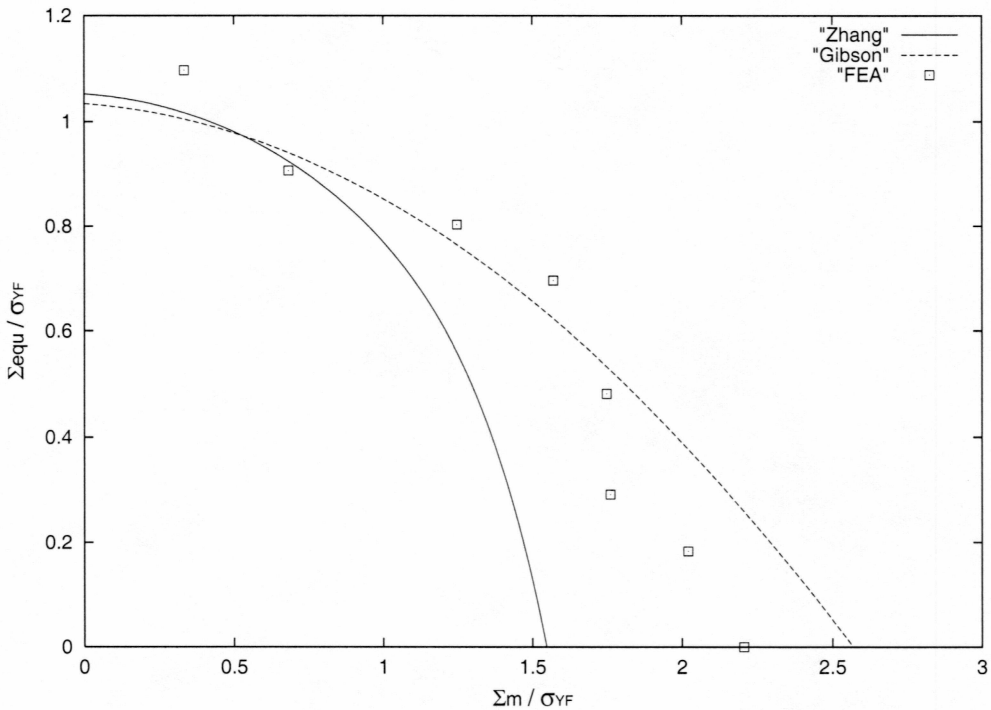

Figure 5.4: Yield surfaces for the unit cell with $f = 0.80$, the FEA surface obtained by using the 0.2% ε_p method

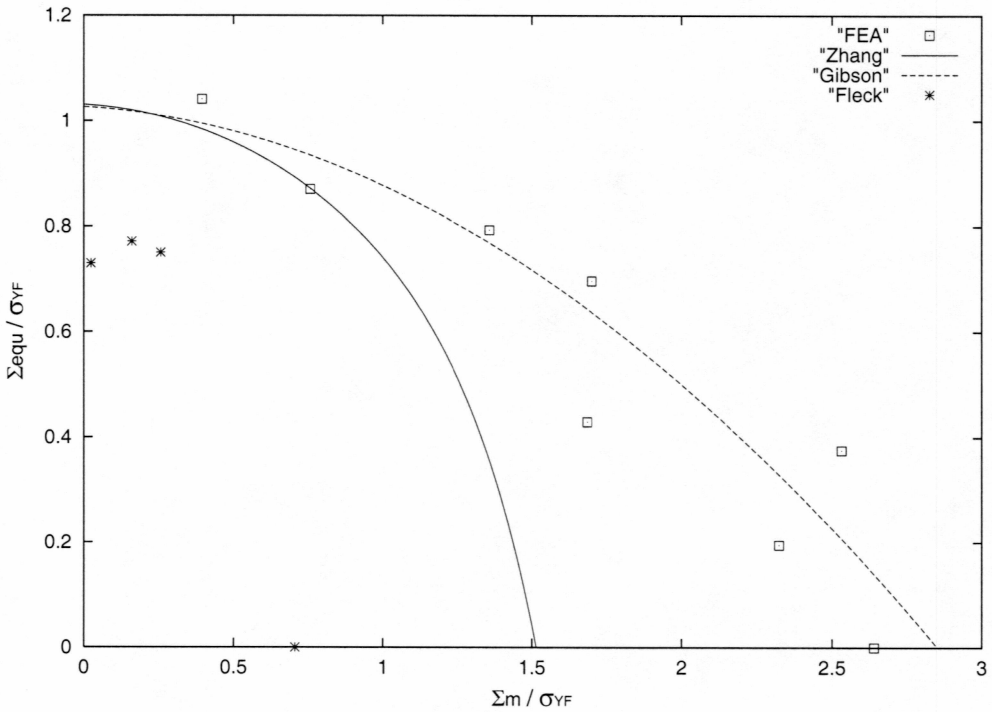

Figure 5.5: Yield surfaces for the unit cell with $f = 0.84$, the FEA yield surface obtained by using the 0.2% ε_p method

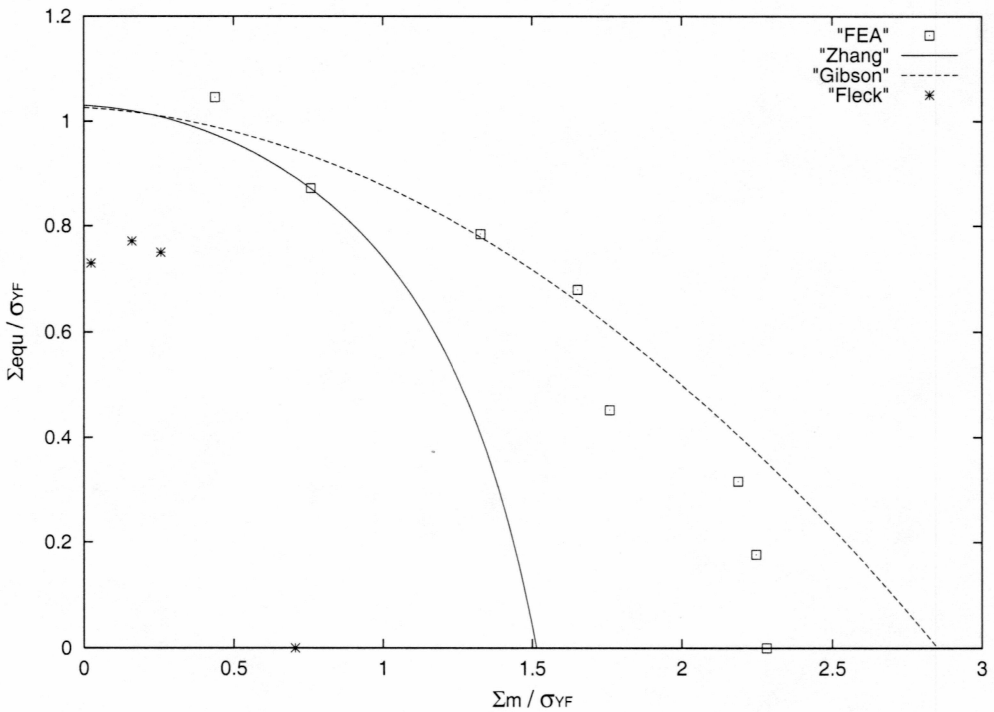

Figure 5.6: Yield surfaces for the unit cell with $f = 0.84$, the FEA yield surfaces obtained by using the 0.5% ε_p method

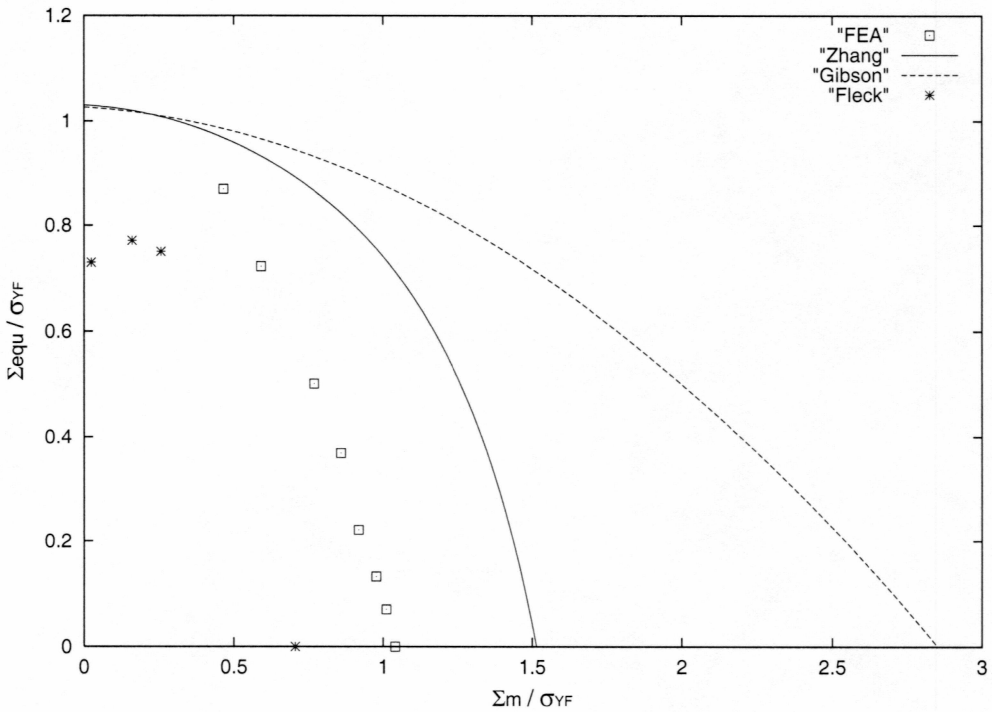

Figure 5.7: Yield surfaces for the unit cell with $f = 0.84$, the FEA yield surface obtained by using the transition point method

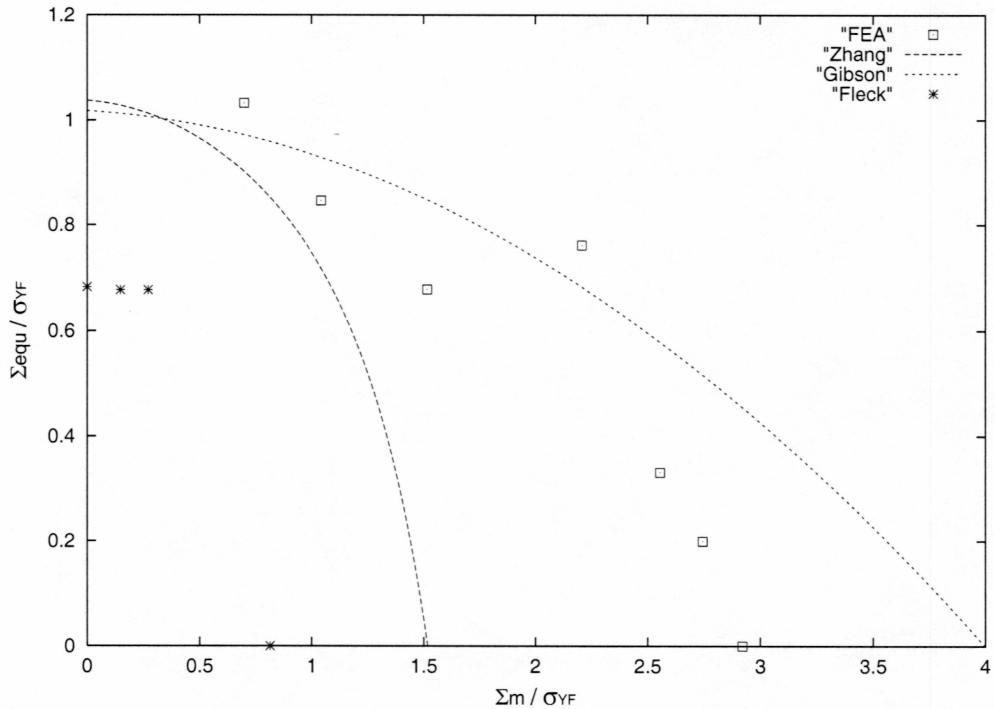

Figure 5.8: Yield surfaces for the unit cell with $f = 0.92$, the FEA yield surface obtained by using the 0.2% ε_p method

Chapter 6

Discussions and conclusions

The goal of this work is to get a better understanding of the yield behavior of foams and to verify Lee and Zhang's theoretical analysis. A kind of very complicated foams using the Kelvin model was selected to investigate. Numerical simulations of the yield behavior of the foams have been conducted using the commercial FEA code ABAQUS. C++ programs were developed to generate three dimensional meshes for unit cells with various void fractions. It greatly facilitated the FEA. Yield surfaces based on FEA were acquired and compared with those obtained from the analytical models and available experimental data. We can make the following conclusions:

(1) Bending is the main mode of deformation of the unit cell under the loading cases we applied. Figure 6.1 to Figure 6.4 are four contours of the equivalent plastic strain (PEEQ in ABAQUS) for the unit cell $f = 0.92$ under loading case 3 ($D_x = 0.42$, $D_y = 0.0$, $D_z = -0.42$). They show the development

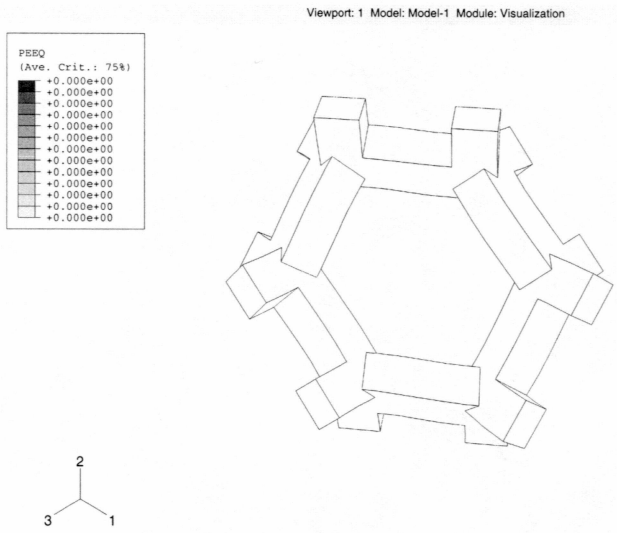

Figure 6.1: The contour of the equivalent plastic strain for the unit cell $f = 0.92$ under loading case 3 ($D_x = 0.42$, $D_y = 0.0$, $D_z = -0.42$), FEA increment 4, no plastic deformation occurs

and distribution of the plastic zone. It can be seen clearly that the plastic deformation first occur at joints (intersections); the plastic deformation is mainly due to bending and stress concentration. As the loading increases, the plastic deformation expands around the joints, and then axial loading also contribute to further deformation, and eventually the necking emerges around the joints on the struts which are almost parallel to the direction of the tension load after deformation.

(2) Void fraction f and the yield strength of a foam wall (or strut) material

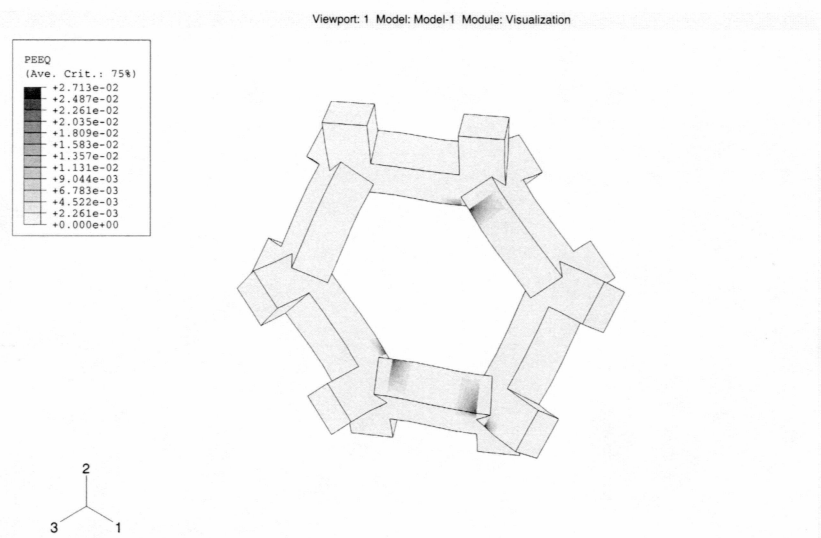

Figure 6.2: The contour of the equivalent plastic strain for the unit cell $f = 0.92$ under loading case 3 ($D_x = 0.42$, $D_y = 0.0$, $D_z = -0.42$), FEA increment 5, plastic deformation first occurs

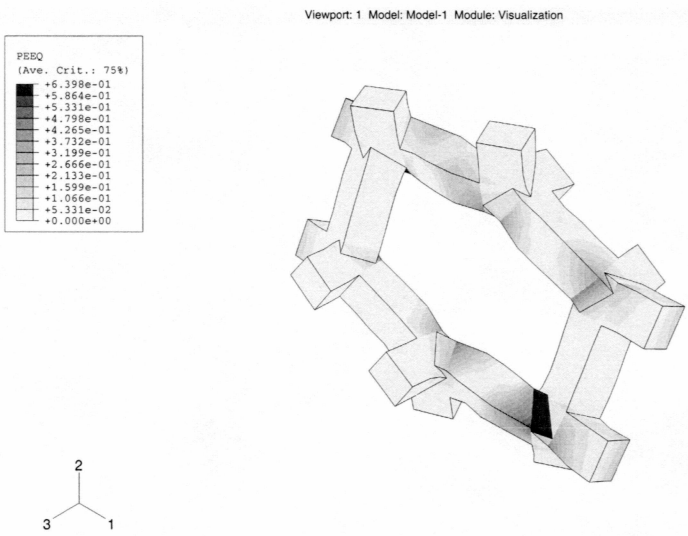

Figure 6.3: The contour of the equivalent plastic strain for the unit cell $f = 0.92$ under loading case 3 ($D_x = 0.42$, $D_y = 0.0$, $D_z = -0.42$), FEA increment 12, plastic deformation expands

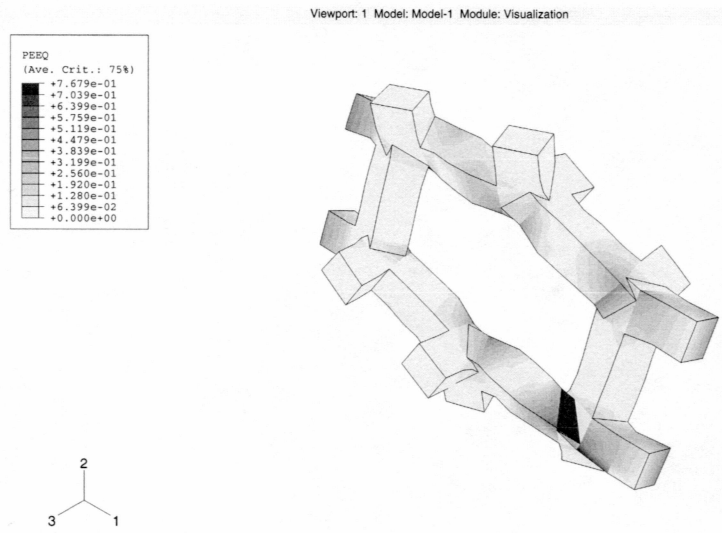

Figure 6.4: The contour of the equivalent plastic strain for the unit cell $f = 0.92$ under loading case 3 ($D_x = 0.42$, $D_y = 0.0$, $D_z = -0.42$), FEA increment 21 (the last one), plastic deformation expands and necking occurs

are not the only factors that affect the yield function of a foam. The geometry and the structure of the foam also have a great effect on its yield behavior. Comparisons between yield surfaces normalized by the uniaxial tensile strength of the foams show good agreements for foams with a certain void fraction f but different structure of unit cells. It can been seen from Figure 5.1 to Figure 5.4. In Lee and Zhang's paper, comparisons between yield surfaces normalized by the yield strength of the strut materials are not very clear and distinct. Therefore it is much more reasonable to do comparisons between yield surfaces normalized by the uniaxial strength of foams.

(3) Comparisons show that Gibson's, Zhang's theoretical results, and our FEA data have good agreements, especially in the area of pure shear – the area close to the axis of normalized equivalent stress shown in Figure 5.1 to Figure 5.8. At the end of hydrostatic end close to the axis of the normalized mean stress, it seems that Gibson's results are overestimated, Zhang's results are conservative, and Fleck's results are even more conservative. Several factors could be attributed to the discrepancies: the rigid-plastic material model is used in the theoretical derivation, the undeformed geometry is used such that large deformation is not considered, the approximations were made in obtaining the velocity field and the plastic energy dissipation rate in Lee and Zhang's model.

(4) It is apparent from Figure 5.7 that the FEA yield surface obtained by using the transition point method is very close to Fleck's experimental data. These methods predict the yield points at which the foams are at failure and

not the initial yield.

The current study does not include the instability analysis and elastic and plastic buckling which may cause the difference between yielding under tensile loading and that under compressive loading.

In the future, the derived yield function will need to be improved. For simplicity, some empirical parameters may be considered to be added into the yield function after acquiring enough numerical and experimental results. The instability analysis and buckling effects should be considered.

Bibliography

[1] ABAQUS, 1999, "User Manual," Version 5.8, Hibbit, Karlson & Sorensen, Inc..

[2] Casey, J. Naghdi, P. M., 1981, "On the Characterization of Strain-Hardening Plasticity," *J. Appl. Mech.* Vol. 48, pp649-653.

[3] Chen, W. F. and Hanm, D. J., 1988, *Plasticity for Structural Engineers*, Springer-Verlag, New York.

[4] Deitel, H. M., & Deitel, P. J., 1998, "*C++ How to Program*", Second Edition, Prentice-Hall, Inc.

[5] Deshpande, V. S. and Fleck, N. A., 2001, "Multi-Axial Yield Behavior of Polymer Foams", Acta mater, 49 (2001) 1859-1866.

[6] Freire, J. L. F. and Riley, W. F., 1980, "Yield behavior of Photoplastic Materials," *Experimental Mechanic*s, Vol. 20, pp. 118-125.

[7] Gibson, L. J., Ashby, M. F., Zhang, J. and Friantafillou, T. C., 1989, "Failure Surfaces For Cellular Materials Under Multiaxial Loads - I. Modeling," *Int. J Mech. Sci.* Vol. 31, No. 9, pp. 635-663.

[8] Grenestedt, Joachim L., 1998, "Influence of Imperfections on Effective Properties of Cellular Solids," *Materials Research Society Symp. Proc.,* Vol. 521.

[9] Gurson, A. L., 1977, "Continuum Theory of Ductile Rupture by Void Nucleation and Growth: Part I – Yield Criteria and Flow Rules for Porous Ductile Media", ASME *J. Eng. Mat. Tech.,* Vol. 99, pp. 2-15.

[10] Jeong, H. -Y. and Pan, J., 1995, "A Macroscopic Constitutive Law for Porous Solids With Pressure-Sensitive Matrices and Its Implications to Plastic Flow Localization," *Int. J. Solids Structures*, Vol. 32, No. 24, pp. 3669-3691.

[11] Kramer, E. J., 1983, "Microscopic and Molecular Fundamentals of Crazing," *Advances in Polymer Science*, pp. 1-56.

[12] Lee, J. H. and Oung, J., 2000, "Yield Functions and Flow Rules for Porous Pressure-Dependent Strain-Hardening Polymeric Materials," *J. Appl. Mech*, Vol. 67, pp. 288-297.

[13] Lee, J. H., 1990, "On the Asymmetry of Elastic-Plastic Moduli for a Class of Pressure-Dependent Models in Strain Space," *Act Mechanica*, Vol. 84, pp. 133-151.

[14] Lee, J. H., 1989, "Characterization of Strain Hardening for a Simple Pressure-Sensitive Plasticity Model," *Acta Mechanica,* Vol. 77, pp. 133-151.

[15] Lee, J. H. 1988, "Upper Bound Analysis of the Upsetting of Pressure-Sensitive Polymeric Rings," I*nt. J. Mech. Sci.*, Vol. 30, pp. 601-612.

[16] Lee, J. H. 1988, "Some Exact and Approximate Solutions for the modified von Mises Criterion." *J. Appl. Mech.,* Vol. 55, pp. 260-166.

[17] Oung, J., 1999, "Yield Functions and Flow Rules for Porous Pressure-Dependent Strain-Hardening Polymeric Materials," M. Sc. Thesis, University of Alaska, Fairbanks, AK.

[18] Raghava, R. S., Caddell, R. M. and Yeh, G. S. Y., 1973, "The Macroscopic Yield Behavior of Polymers," *Journal of Materials Science*, Vol. 9, pp. 225-232.

[19] Reddy, J. N., 1994, "*An Introduction to the Finite Element Method*," Second Edition, McGraw-Hill, Inc.

[20] Spitzig, W. A. and Richmond, O., 1979, "Effect of Hydrostatic Pressure on the Deformation Behavior of Polyethylene and Polycarbonate in Tension and Compression," *Poly. Eng. Sci.*, Vol. 19, pp. 1129-1139.

[21] Thomson, W. (Lord Kelvin), 1887, "On the Division of Space with Minimum Partitional Area," *Phil. Mag.*, Vol. 24, No. 151, pp. 503 - 514.

[22] Theocaris, P. S., 1989, "The Paraboloid Failure Surface for the General Orthotropic Material, " *Acta Mechanica* Vol. 79, pp. 53-79.

[23] Timoshenko and Goodier, 1969 "*Theory of Elasticity*," third Edition, McGraw-Hill Inc..

[24] Trantafilllou, T. C., and Gibson, L. J., 1990, "Multiaxial Failure Criteria For Brittle Foams," *Int. of Mesh. Sci.* Vol. 32, No. 6, pp. 479-490.

[25] Triantafillou, T. C., Zhang, J., Shercliff, T. L., Gibson, L. J. and Ashby, M. F., 1989, "Failure Surfaces For Cellular Materails Under Multiaxial Loads - II. Comparison of Models with Experiment," *Int. J. Mech. Sci.* Vol. 31, No. 9, pp. 665 - 678.

[26] Tvergaad, V., 1990, "Material Failure by Void Growth to Coalescence," *Advances in Applied Mechanical*, Vol. 27, pp. 83-151.

[27] Wolfram, S. 1994, *Mathematica: The Student Book,* Addison-Wesley Publishing Company.

[28] Xu, J., 1998, "Finite Element Analysis of Porous Pressure-Dependent Polymeric Materials, M. Sc., Thesis, University of Alaska Fairbanks.

[29] Zhang, T., Lee, J. H., 2002, "A plasticity Model for Cellular Materails with Open-Celled Structure", accepted to publish in *Int. J. of Plasticity.*